IMPLEMENTATION OF DAMAGE MODEL FOR CERAMICS

M.Tech Thesis

by

CHANDRA PRATAP SINGH

DEPARTMENT OF MECHANICAL ENGINEERING

INDIAN INSTITUTE OF TECHNOLOGY INDORE MAY 2025

IMPLEMENTATION OF DAMAGE MODEL FOR CERAMICS

M.Tech Thesis

Submitted in partial fulfillment of the

requirements for the award of the degree

of

Master of Technology

by

CHANDRA PRATAP SINGH

(2302103035)

Under Supervision of

Dr. MAYANK CHOUKSEY

&

Dr. INDRASEN SINGH

DEPARTMENT OF MECHANICAL ENGINEERING

INDIAN INSTITUTE OF TECHNOLOGY INDORE

MAY 2025

INDIAN INSTITUTE OF TECHNOLOGY INDORE

CANDIDATE'S DECLARATION

I hereby certify that the work which is being presented in the thesis entitled "**Implementation of Damage Model for Ceramics**" in the partial fulfillment of the requirements for the award of the degree of **MASTER OF TECHNOLOGY** and submitted to the **DEPARTMENT OF MECHANICAL ENGINEERING, Indian Institute of Technology Indore**, is an authentic record of my own work carried out during the time period from May 2024 to May 2025 under the supervision of **Dr. Mayank Chouksey**, & **Dr. Indrasen Singh**, Assistant Professor, Department of Mechanical Engineering, Indian Institute of Technology Indore.

The matter presented in this thesis has not been submitted by me for the award of any other degree of this or any other institute.

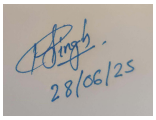

Chandra Pratap Singh

(Student)

This is to certify that the above statement made by the candidate is correct to the best of my knowledge.

Dr. Mayank Chouksey

(Thesis Supervisor)

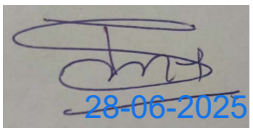

Dr. Indrasen Singh

(Thesis Co-Supervisor)

Mr. Chandra Pratap Singh has successfully given his M.Tech Oral Examination held on May 23, 2025.

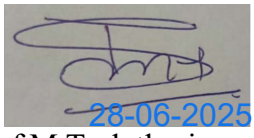

Signature of Supervisor(s) of M.Tech thesis

Date:

Convener, DPGC

Date: 29-06-2025

ACKNOWLEDGEMENTS

I am profoundly grateful to my supervisors, Dr. Mayank Chouksey and Dr. Indrasen Singh, for their exceptional guidance, unwavering support, and encouragement throughout my M.Tech journey. Your insightful advice, extensive knowledge, and continuous motivation were crucial in the completion of this project. I deeply appreciate your dedication to my academic and personal growth.

I would like to express my sincere gratitude to my final exam committee members Prof. Anand Parey, Dr. Krishna Mohan Kumar. Their thorough review, and constructive, and insightful suggestions have greatly refined and elevated the quality of this thesis. I deeply appreciate their time and effort in evaluating my work and providing valuable feedback.

I would also like to extend my heartfelt thanks to my group mates at the Computational Solid Mechanics (CSM) Lab. Their friendship and collaboration have been indispensable throughout this journey. Our discussions and shared experiences have made this journey productive and enjoyable. Above all, I am deeply grateful to my beloved parents for their unconditional love, support, and encouragement throughout this journey. Their belief in me has been a constant source of strength and motivation.

ABSTRACT

This thesis presents the development and implementation of a micromechanics-based damage model for ceramics subjected to high strain rate loading. Advanced ceramics, owing to their exceptional thermal, mechanical, and chemical properties, are widely used in critical applications such as defence, aerospace, and biomedical industries. However, their brittle nature and sensitivity to flaw-induced failure demand robust constitutive models to predict fracture behaviour under dynamic conditions.

A modified framework extending the ref. [19] model has been formulated, incorporating a rate-sensitive crack growth law to account for loading-rate-dependent fracture toughness. The model captures the initiation and growth of wing cracks under compressive stress states and links microcrack evolution to macroscopic behaviour through a representative population of flaws. Implementation of this model is achieved in MATLAB for uniaxial and hydrostatic compression cases.

Comparative analysis with experimental data from Dionysus-Pentelicon marble validates the model's ability to replicate the strain-rate sensitivity and damage evolution observed in brittle materials. The work highlights the model's potential in accurately forecasting failure in ceramics under dynamic loading, and suggests improvements for capturing post-peak softening and local damage instabilities.

TABLE OF CONTENTS

Table of Contents

LIST OF FIGURES

NOMENCLATURE

σ_1	Largest compressive stress (MPa).
σ_2, σ_3	Smaller principal compressive stress (MPa).
σ, τ	Normal and shear stress on crack plane.
σ_{xy}	Shear stress acting in crack plane (MPa).
$2a$	Length of initial angled crack(m).
l	Extension of wing crack(m).
L	Dimensionless wing crack length $(L = l/a)$.
b	Sample thickness.
t	Width of beam or column.
ψ	Angle between σ_1 and crack face.
θ	Angle measured from crack plane.
E_0	Young's modulus of the uncracked body.
E	Young's modulus of the crack body (MPa).
K_I	Mode I stress intensity $(MPa\ m^{\frac{1}{2}})$.
K_{IC}	Mode I fracture toughness.
u_s	Crack sliding displacement.
$2\delta n$	Mode I crack opening displacement at mid-point(m).
$2\delta s$	Mode II sliding displacement at mid-point(m).
$2\delta t$	Net mode I crack opening displacement at midpoint.
T_n, T_s	Traction acting on crack surfaces (MPa).
G	Strain energy release rate(m^{-2}).
μ	Co-efficient of friction.
U, UI, UII	Elastic energy stored in crack fields (J).
W	Work done by applied stresses (J).
N_A	Number of cracks per unit area (m^{-2}).
λ	Ratio of principal stresses(σ_3/σ_1).
σ_y	Yield strength (MPa).
$\alpha_1, \alpha_2, \alpha$	Dimensionless constants.
β_b, β_s	Dimensionless constants.

Chapter 1

Introduction

1.1 Ceramics

The word "ceramics" originates from the Greek term "keramos" which means potter's clay. The essential properties of ceramics include their durability along with their versatility and visual appeal in products such as porcelain and earthenware. Ceramics form when clay mixes with water and minerals including silica and alumina and feldspar while metal oxides serve as important components. Advanced ceramics such as zirconia and tungsten carbide incorporate carbon, nitrogen and sulfur compounds to fulfill industrial requirements. Oxide ceramics consist of metallic and metalloid components whereas non-oxide ceramics including nitrides, carbides and borides provide outstanding hardness and conductivity. The composition is adjusted to produce desired properties which enables multiple applications in artistic works and technological systems and industrial processes. The final product characteristics determine the specific formulation of ceramics. Ceramic products exist in two forms because pure clay is used for some making while silica and feldspar enhance others with additional properties. Advanced materials such as zirconia and tungsten carbide are produced for specific industrial functions.

1.2 Properties of Ceramics

Bond: The remarkable strength and stability of ceramics exist because their atomic structure contains both covalent and ionic bonds. Ceramic materials develop a sturdy lattice structure through their bonding connections that makes them resistant to deformation forces.

Strength: Ceramics provide significant strength for rigid applications but metals generally possess higher tensile and compressive strength. The strength-per-weight value of ceramics proves useful in particular engineering tasks.

Brittleness: Ceramics break easily because they lack elasticity so that stress leads to fractures without much plastic deformation. The brittleness of ceramics creates an obstacle in situations that require both toughness and hardness.

Electrical connectivity: The ionic or covalent bonds within ceramics prevent free electron movement which results in restricted electrical flow. Ceramics demonstrate their effectiveness as electrical insulators throughout various engineering applications because of their specific electrical properties.

Thermal conductivity: Ceramics serve their purpose well in both thermal insulation applications and high temperature environments because they possess poor thermal conductive properties. The combination of high heat resistance and low thermal conductivity enables ceramics to withstand temperature extremes which makes them suitable for engine and furnace applications.

Density: The physical characteristics of ceramics stem from their density which stands between the densities of metals and polymers. The material choice for specific situations might be affected by this property. Ceramics provide a beneficial combination of low weight and high strength for applications which require equilibrium between these two factors such as aeronautical components.

1.3 Application of Ceramics

Electronics

Manufacturing electronic parts like capacitors, resistors and IC substrates uses ceramics extensively in the industry. The use of ceramics in piezoelectric devices enables precise electrical signal generation for sensor and actuator applications and ultrasound machines.

Automotive Industries

Ceramics find applications in automotive industry engine production because they can withstand high temperatures and corrosive environments. Ceramic-coated automotive parts provide enhanced wear resistance along with reduced engine friction which results in better engine performance and fuel economy.

Aerospace & Defence

Ceramics play a crucial role in aerospace and defence industries through their use in developing lightweight aircraft engine components and missile nose cones and heat shields because of their strong weight-to-strength ratio and ability to handle extreme temperatures. The military uses armour plating made of ceramics to protect personnel and vehicles because of their strong ballistic resistance.

Medical Applications

Ceramics play a crucial role in medical applications because of their biocompatibility and resistance to physiological fluids which allows them to create orthopaedic implants such as hip and knee replacements and dental implants and surgical instruments. Medical professionals use bioactive ceramics to promote bone regeneration during tissue engineering as well as bone grafting procedures.

Chapter 2

Literature Review & Problem Statement

2.1 Literature review

The story of understanding brittle material failure, like ceramics, rocks, and ice, unfolds through decades of research, each study revealing new facets of how cracks lead to catastrophe. In 1963, Brace and Bombolakis [32] noted that the stress to start cracks in compression differs from that causing final fracture. By 1964, Walsh and Brace [40] explored ceramics under tension and compression, finding Griffith's theory apt for tension but inadequate for compression due to crack closure.

In 1991, Schulson's [41] team studied ice, showing cracks nucleate at grain scales (1-10 mm) and grow under confinement, with fracture stress rising sharply at low confinement. Following ref. [39] found that damage in Westerly granite deviated from earlier predictions, underscoring the need for models capturing progressive micro-failure ref. [16] revealed that cracks near surfaces grow faster, laying groundwork for damage mechanics, while ref. [20] refined this model for rocks, focusing on crack interactions.

From ref. [26] we identified three deformation regimes—quasi-static, intermediate, and high-velocity—tying loading rate to ceramic failure. Finally, ref. [20] developed a micromechanics model for high-speed crack propagation, fitting rock failure surfaces and simulating earthquake dynamics.

Earlier studies oversimplified crack interactions, misapplied Griffith's theory to compression, and neglected dynamic loading and microstructural complexity. These gaps point to future research in dynamic crack growth and grain-scale effects.

2.2 Failure Mechanisms of Ceramics

Ceramics generally fail due to their brittle nature and low fracture toughness. The failure mechanism of brittle fracture [42] occurs when microcracks or pores or surface flaws concentrate stress until sudden breakage happens. Thermal shock [43] causes cracks to develop because of quick temperature variations which create thermal stress within materials. The combination of cyclic loading [44] and moisture exposure leads to subcritical crack development which results in fatigue failure. High-temperature environments [45] cause ceramics to deform over time through grain boundary sliding and viscous flow

mechanisms. In this thesis we will be focusing on brittle fracture of ceramic material under different loading condition. From ref. [32] performed some experiments to investigate growth of cracks in photo elastic material and glass under uniaxial compression.

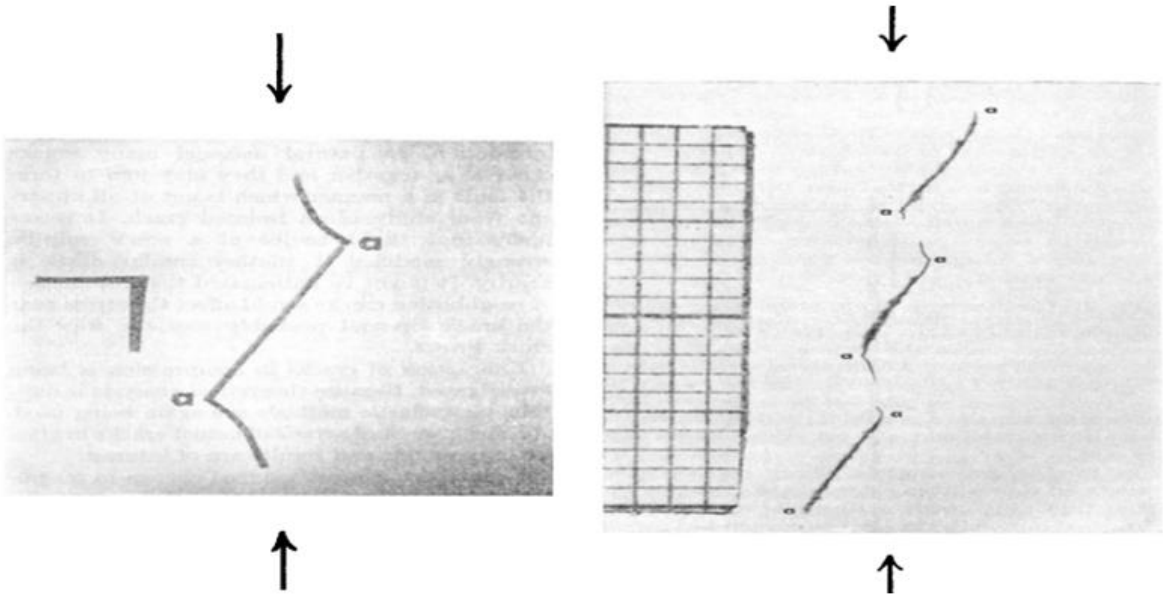

Fig. 2. 1: (a) Result of actual crack growth in photo-elastic plastic.
(b) Growth of an array of cracks in glass (taken from ref. [32])

Comparing crack behaviour in ceramics under tension and compression reveals distinct patterns. In tension, a critical crack, once initiated, propagates along its long axis until it reaches a free boundary, often forming a macroscopic crack from a single preexisting flaw. In compression, however, a growing crack deviates from its initial long axis, curves toward the compression direction, and halts after traveling a short distance (a few crack lengths).

Wing cracks emerge from inclined flaws due to shear stress-induced sliding, creating tensile stress concentrations at crack tips (Fig. 2.2). Cracks aligned parallel or perpendicular to the applied stress experience no shear stress and theoretically do not extend. As stress increases from zero, a critical tensile stress triggers wing crack initiation, leading to growth into the tensile zone.

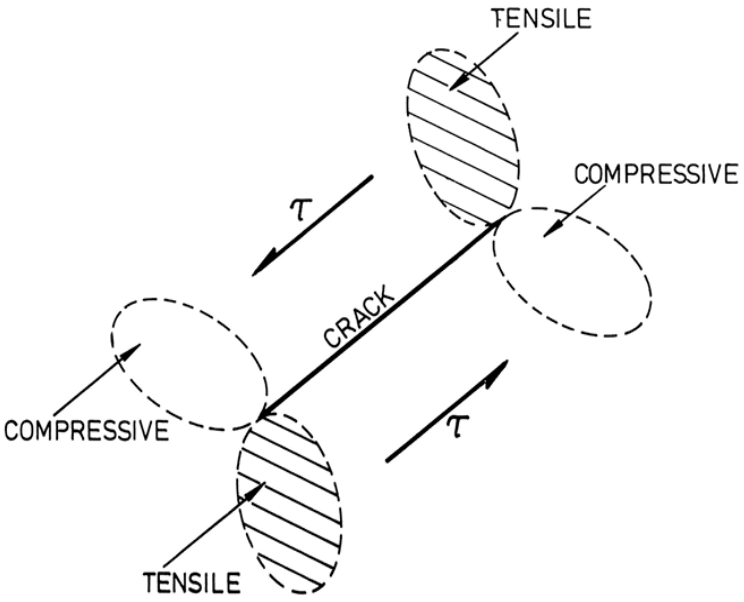

Fig. 2. 2: Shear stresses acting on the angled cracks generate zones of concentrated tensile stress at the crack tip (taken from ref. [31])

2.3 Problem Statement

This project aims to develop and numerically implement a micromechanics-based damage model for ceramics, focusing on the wing crack mechanism, to enhance the understanding and prediction of their failure behavior under compressive loading and high strain rates. Previous studies failed to adequately distinguish between compressive and tensile stress regimes & transition between them. Also, prior model insufficiently addressed high strain rate loading relevant to rapid failure events. Following are the key objectives:

- Implement a micromechanics-based damage model using numerical calculations in MATLAB.
- Introduce scalar damage parameter D to describe the evolution of micro-crack growth, accounting for the size and density of cracks under compressive and tensile stress regimes
- Determine the optimal parameter ranges that accurately fits experimental failure surfaces (σ_1, σ_3) for a range of rocks and capturing the onset of nonlinearity in stress-strain curves.
- Accurately capture the initiation and growth of wing cracks in ceramics under different loading states.

2.4 Experimental studies of Ceramic failure

In the strain-rate range of 10^2–10^4 s^{-1}, the Split Hopkinson Pressure Bar (SHPB) is a key dynamic testing tool that employs 1D wave propagation to evaluate material constitutive properties under tension, compression, and torsion ref. [34] offer a comprehensive review of the technique, with further insights provided by studies like ref.[35-38] primarily focusing on ductile materials.

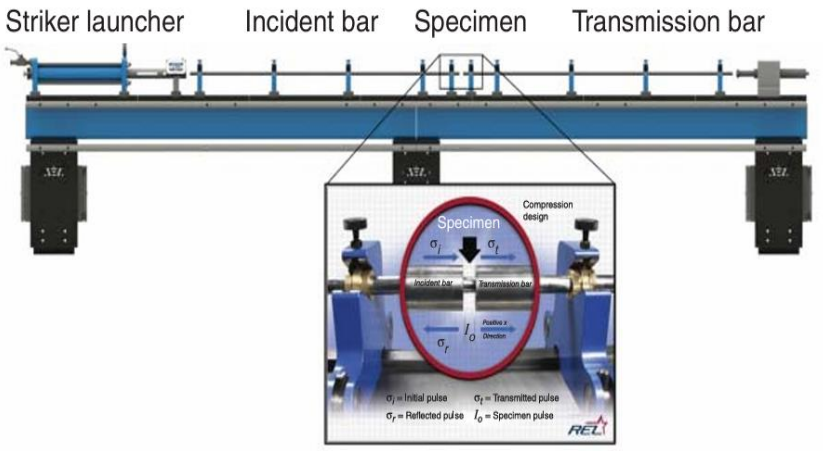

Fig. 2. 3 : A Split Hopkinson pressure bar made from maraging steel. The magnified view illustrates the specimen held between the two bars (Source: Courtesy of REL Inc, Calumet MI, USA.)

Chapter 3
Constitutive Modeling

3.1 Ceramic Modeling

Modeling ceramic materials depends on the intended application—structural analysis, thermal response, fracture behavior, or multi-physics coupling—and the scale of interest (microscale, macroscale, continuum). The common approaches to model ceramics are listed below.

3.1.1 Continuum Damage Mechanics Model

In continuum damage mechanics (CDM), the stress-strain relation for ceramics is expressed as [1-2]

$\sigma = E_e \varepsilon$; where $E_e = E_0(1 - D)$

Here, $D = 0$ indicates an undamaged state, and $D = 1$ denotes complete local failure. The damage measure D can be a scalar, vector, or tensor (second or higher rank) reflecting varying complexity. Approaches to determine effective properties (e.g., E_e, Poisson's ratio) for solids with non-periodic defects fall into three categories: numerical models, analytical models and empirical models. Numerical models handle diverse shapes but demand high computational resources. Analytical models study defect arrangements but are limited to regular shapes (e.g., spherical, ellipsoidal) due to available elasticity solutions. Empirical models fit experimental data but lack universality.

3.1.2 Analytical Models

Analytical models are used for determining effective properties of porous ceramics, developed within small-deformation linear elasticity, predict macroscopic behaviour from microstructural parameters. Analytical models are effective for simple geometries and low porosity, common models include self-consistent [3], differential [4], Mori-Tanaka [5], composite sphere [6], and minimum solid area models [7]. These involve: (1) determining stress and strain distributions for a matrix-inclusion geometry, and (2)

adjusting for inclusion interactions. With regard to the second step, it can be divided into two categories: non-interacting and interacting models.

Non-interacting models assume independent pores, valid only for low porosity, while interacting models account for pore and crack interactions.

3.1.3 Numerical Models

Numerical models for heterogeneous ceramics use random or digital representations, modeled as spring networks or finite elements. Random representations generate microstructures statistically, while digital ones use computed tomography (CT), X-ray, or SEM images. The microstructure is discretized into elements, and elasticity equations are solved via finite element methods (FEM) using variational formulations, minimizing elastic energy with techniques like the fast conjugate gradient method. Periodic boundary conditions are assumed, yielding results as simple two- or three-parameter relations that link properties to porosity. Studies have explored porosity's impact on Young's modulus, Poisson's ratio, and thermal conductivity, but often overlooked pore size, shape, and number due to complexity. Tsukrov and Novak [9] have combined numerical and analytical approaches, solving defect-specific elasticity problems numerically within linear elasticity, accounting for shape, size, and porosity, but neglecting nonlinear effects like hole closure under compression.

3.1.4 Damage Evolution

Damage variables in ceramics evolve with stress and strain, causing new cracks or damage. Damage evolution rules are derived via three methods: experiment-based [10], micromechanical [11], and thermodynamics-based [12]. Experiment-based methods, using curve fitting yield reliable results for tested cases but lack generalizability. Micromechanical methods derive microcrack growth laws, but are limited to homogeneous, linear isotropic solids without crack interactions.

Thermodynamics-based methods include: (1) associated methods, defining a damage surface with evolution normal to it, ensuring state variables align with successive surfaces; (2) non-associated methods; and (3) direct methods.

The non-associated method relaxes these constraints, allowing flux and consistency from different surfaces, e.g., linking damage to Von Mises equivalent strain. The direct method uses thermodynamic

principles like Onsager relations or a dissipation function to deduce damage evolution via differential relations.

3.2 Fracture Mechanics & Micromechanical Models

3.2.1 Fracture Mechanics

In fracture mechanics (FM), macrocrack growth is explicitly modeled, with unstable crack length increase under tensile stress in a homogeneous microstructure. In linear fracture mechanics, cracks are idealized as sharp-tipped, two-dimensional defects in a linear, isotropic elastic solid, exhibiting perfectly brittle failure. Unlike three-dimensional flaws like pores with finite radii, cracks have zero-radius tips. Crack extension is described by two equivalent approaches: Griffith's energy approach [13] and Irwin's stress approach [14].

$$G_I = \frac{K_I^2}{E}$$

$$\sigma_{ij} = \frac{K_I}{\sqrt{2\pi r}} f_{ij}(\theta)$$

where G is called "the energy release rate", K is called "the stress intensity factor", the subscript I represents loading mode I, E is the Young's modulus, $f_{ij}(\theta)$ are known angular functions, σ_{ij} are stresses near the crack tip and r is the distance from the crack tip.

3.2.2 Micromechanical Models

As discussed in the sections above, FM approaches can be used to study the growth of the macrocrack through a solid with a heterogeneous microstructure, while CDM approaches can be used to determine the continuum damage accumulation that occurs before the macrocrack. The distinction lies in crack scale: microcracks (CDM) versus macrocracks (FM), with the surrounding medium's scale being critical. Classical parameters like stress intensity factor K_I or energy release rate G rely on local theory, but global behavior and crack interactions require non-local approaches. A local CDM-FEM approach aids elastic-brittle fracture analysis. Micromechanical models bridge micro- to macroscale, using FM or CDM to derive effective constitutive relations by explicitly modeling microstructural features (e.g., microcrack evolution, coalescence). These models capture arbitrary morphologies, stochastic fracture patterns, and natural crack initiation, growth, and coalescence under loading [8].

Direct microscale discretization via finite element methods is challenging due to random defect distributions (size, location) and high computational demands. Micromechanical models use a representative volume element (RVE), sized to include sufficient microvoids or microcracks while maintaining near-homogeneous stress-strain fields. RVE microstructure is modeled via digital image-based methods (e.g., micro-CT or CCD camera images, processed numerically) or random methods, where void/pore properties are statistically generated based on 2D observations (porosity, morphology). Subsequent steps involve selecting numerical techniques to solve boundary-value problems and defining constituent constitutive equations.

3.3 Multiscale Analysis

Finite element methods (FEM) are widely used in structural stress analysis and fracture mechanics, typically assuming material homogeneity. However, heterogeneous materials like ceramics, with microscale defects (cracks, voids, pores, inclusions), require multiscale models [15] to link microstructure to macroscopic behavior. Unlike single-scale local models, multiscale models are gradient-based or nonlocal, considering stress at a point as dependent on local strain, its spatial derivatives, or strains in a surrounding region. For example, a multilevel model for composites and porous materials uses Voronoi cell FEM for microstructural analysis and conventional FEM for macroscale, coupled via asymptotic homogenization. A three-scale model integrates microstructure, macrostructure, and fracture origins (e.g., cracks) using homogenization and FEM mesh superposition, effectively analyzing non-periodic microscopic stresses at crack tips under non-uniform strain fields. Other models combine FM or CDM with mesh superposition for crack propagation, while statistical approaches or Monte Carlo FEM predict elastic constants and fracture scatter in thin films.

3.4 Wing Crack Model

The wing crack model is a micromechanical approach to describe the propagation of cracks in brittle materials under compressive loading. It specifically addresses how pre-existing microcracks, often oriented at an angle to the applied compressive stress, initiate tensile wing cracks at their tips. Brittle materials like ceramics usually contains very small cracks due to defects, surface irregularities & micro porosity. When loaded under compression the crack interactions lead to macroscopic failure of the materials. Unlike the macroscopic models (e.g. Mohr-Coulomb criterion), which uses bulk properties of

the material, the wing crack model considers discrete microstructural features, such as crack geometry & local stress concentrators. The wing crack model is a powerful micromechanical tool that addresses the limitations of conventional theories by focusing on single crack propagation and stress intensity factors.

3.5 Initiation & growth of wing cracks in plate in compression

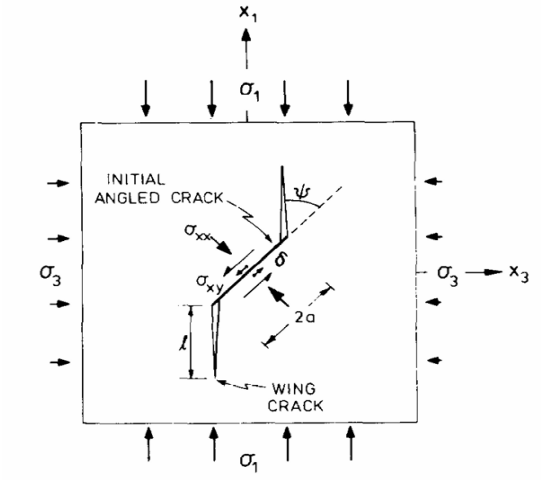

Fig. 3. 1: Schematic of wing crack growth from an angled crack under a compressive stress σ_1 (taken from ref. [16])

The growth of wing cracks from sharp starter flaws is shown in Fig. 3.1, when an incremental compressive load is applied vertically. First, we will talk about initiation & growth of wing cracks from starter flaws then we will discuss about the crack interactions & influence of material parameters like Poisson's ratio, inclination angle in crack growth. The discussion in this section is taken from ref. [16].

Considering an infinite elastic plate containing an initial crack of length 2a & subjected to principal stresses σ_1 & σ_3. Stresses are treated as positive when tensile, negative when compressive.

σ_1 = Most negative (Most Compressive)

σ_3 = Most positive (Least Compressive)

The remote stress field generates in plane shear stress, σ_{xy} and normal stress σ_{xx} which are given by ref. [16]:

$$\sigma_{xy} = \left(\frac{\sigma_3-\sigma_1}{2}\right) sin2\psi = \tau\, sin2\psi, \quad (1)$$

$$\sigma_{xx} = \left(\frac{\sigma_3+\sigma_1}{2}\right) + \left(\frac{\sigma_3-\sigma_1}{2}\right) cos2\psi = \sigma + \tau\, cos2\psi \quad (2)$$

The shear stresses tend to make the crack surfaces slide, but because the crack is closed a frictional stress $\mu\sigma_{xx}$ opposes the sliding. Then effective sliding stress can be expressed as by ref. [16]:

$$\sigma'_{xy} = \sigma_{xy} + \mu\sigma_{xx} \quad (3)$$

The tensile stress $\sigma_{\theta\theta}$ at a distance r from the tip at an angle θ to the crack plane is by ref. [24],

$$\sigma'_{\theta\theta} = \frac{3}{2}\frac{\sigma'_{xy}\sqrt{\pi a}}{\sqrt{2\pi r}}\, sin\theta cos\theta/2 \quad (4)$$

Following ref. [23], the stress intensity K_I on a very small wing crack of length l and oriented at an angle θ to the main crack may be approximated by $\sigma'_{\theta\theta}\sqrt{\pi l}$ at $r = l/2$. Thus, invoking Eq. (4), K_I can be written by ref. [24]:

$$K_I = \frac{3}{2}\sigma'_{xy}\sqrt{\pi a} sin\theta cos\theta/2 \quad (5)$$

The orientation of wing crack corresponding to maximum stress intensity factor can be determined by setting $\frac{dK_I}{d\theta} = 0$, as [24]:

$$\frac{dK_I}{d\theta} = \frac{3}{2}\sigma'_{xy}\sqrt{\pi a}\left[\frac{cos\theta cos\theta}{2} - \frac{\frac{1}{2}sin\theta sin\theta}{2}\right] = 0 \quad (6)$$

Which implies that

$$[cos\theta cos\theta/2 - 1/2\, sin\theta sin\theta/2] = 0$$

$$\theta_c = 70.5°$$

Maximizing K_I with respect to θ gives $\theta_c = 0.392\pi = 70.5$ so that the stress intensity for the wing crack initiation is,

$$K_I = \frac{2}{\sqrt{3}}\sigma'_{xy}\sqrt{\pi a} \quad (7)$$

The most dangerous crack is that lying at the angle ψ which again maximizes K_I. Substituting for σ'_{xy} & maximizing K_I with respect to ψ gives from ref. [16]:

$$K_I = \frac{2}{\sqrt{3}}(\sigma_{xy} + \mu\sigma_{xx})\sqrt{\pi a} \quad (8)$$

$$K_I = \frac{2}{\sqrt{3}}\left[\left(\frac{\sigma_3 - \sigma_1}{2}\right) sin2\psi + \mu\left(\left(\frac{\sigma_3 + \sigma_1}{2}\right) + \left(\frac{\sigma_3 - \sigma_1}{2}\right) cos2\psi\right)\right]\sqrt{\pi a}$$

$$\frac{dK_I}{d\psi} = \frac{2}{\sqrt{3}}\left[\left(\frac{\sigma_3-\sigma_1}{2}\right) 2cos2\psi + \mu\left(\frac{\sigma_3-\sigma_1}{2}\right) - 2sin2\psi\right]\sqrt{\pi a}$$

$$\left[\left(\frac{\sigma_3-\sigma_1}{2}\right) 2cos2\psi - \mu\left(\frac{\sigma_3-\sigma_1}{2}\right) 2sin2\psi\right] = 0$$

$$tan2\psi = \frac{1}{\mu} \tag{9}$$

Now, we know from equation (8) by ref. [16]:

$$K_I = \frac{2}{\sqrt{3}}(\sigma_{xy} + \mu\sigma_{xx})\sqrt{\pi a}$$

from equation (1) & (2),

$$\sigma_{xy} = \left(\frac{\sigma_3-\sigma_1}{2}\right) sin2\psi = \tau\, sin2\psi$$

$$\sigma_{xx} = \left(\frac{\sigma_3 + \sigma_1}{2}\right) + \left(\frac{\sigma_3 - \sigma_1}{2}\right) cos2\psi = \sigma + \tau cos2\psi$$

Substituting equation (1) & (2) in (8) gives [16]:

$$K_I = \frac{2}{\sqrt{3}}\sqrt{\pi a}\left[\left(\frac{\sigma_3-\sigma_1}{2}\right) sin2\psi + \mu\left(\left(\frac{\sigma_3+\sigma_1}{2}\right) + \left(\frac{\sigma_3-\sigma_1}{2}\right) cos2\psi\right)\right] \tag{10}$$

From equation (9) we get [16]:

$$tan2\psi = \frac{1}{\mu}$$

$$\mu = \frac{cos2\psi}{sin2\psi}$$

Substituting these values in equation (10) gives [16]:

$$K_I = \frac{\sqrt{\pi a}}{\sqrt{3}}\left[(\sigma_3 - \sigma_1)sin2\psi + \mu\big((\sigma_3 + \sigma_1) + (\sigma_3 - \sigma_1)cos2\psi\big)\right]$$

$$= \frac{\sqrt{\pi a}}{\sqrt{3}}[(\sigma_3 - \sigma_1)(sin2\psi + \mu cos2\psi) + \mu(\sigma_3 + \sigma_1)]$$

$$K_I = \frac{\sqrt{\pi a}}{\sqrt{3}}\left[(\sigma_3 - \sigma_1)(1 + \mu^2)^{\frac{1}{2}} + \mu(\sigma_3 + \sigma_1)\right]$$

$$K_I = \frac{\sqrt{\pi a}}{\sqrt{3}}\sigma_1\left[\left(\frac{\sigma_3}{\sigma_1} - 1\right)(1 + \mu^2)^{\frac{1}{2}} + \mu\left(\frac{\sigma_3}{\sigma_1} + 1\right)\right]$$

We know this condition is valid only for proportional loading. Considering $\sigma_3 = \lambda\sigma_1$, where λ is ratio of the principal stresses.

$$K_I = \frac{\sqrt{\pi a}}{\sqrt{3}}\sigma_1\left[\left(\frac{\sigma_3}{\sigma_1} - 1\right)(1+\mu^2)^{\frac{1}{2}} + \mu\left(\frac{\sigma_3}{\sigma_1} + 1\right)\right]$$

Thus, K_I can be expressed in terms of λ as [16] :

$$K_I = \frac{\sqrt{\pi a}}{\sqrt{3}}\sigma_1\left[(\lambda - 1)(1+\mu^2)^{\frac{1}{2}} + \mu(\lambda + 1)\right]$$

$$K_I = -\frac{\sqrt{\pi a}}{\sqrt{3}}\sigma_1\left[(1 - \lambda)(1+\mu^2)^{\frac{1}{2}} - \mu(1 + \lambda)\right] \quad (11)$$

The condition for crack initiation is determined by setting K_I equal to K_{IC} (the fracture toughness of material) which results in [16]:

$$\frac{\sigma_1\sqrt{\pi a}}{K_{IC}} = -\frac{3}{\left[(1-\lambda)(1+\mu^2)^{\frac{1}{2}} - \mu(1+\lambda)\right]} \quad (12)$$

This result holds provided σ_{xx} is compressive. When it is tensile, the crack faces separate and the frictional force $\mu\sigma_{xx}$ disappears; but σ_{xx} as well as σ_{xy} is now concentrated by the crack, giving a new term in the equation for the stress intensity.

The stress $\sigma_{\theta\theta}$ at a distance r from the crack tip on the plane at angle θ to the crack plane can be written as [24]:

$$\sigma_{\theta\theta} = -\frac{3\sigma_{xy}\sqrt{\pi a}}{2\sqrt{2\pi r}} sin\theta cos(\theta/2) - \frac{\sigma_{xy}\sqrt{\pi a}}{\sqrt{2\pi r}} cos^3(\theta/2) \quad (13)$$

And substituting eq. (1) & (2),

$$\sigma_{xy} = \tau sin2\psi, \;\; \sigma_{xx} = \sigma + \tau cos2\psi$$

$$K_I = -\frac{3\sqrt{\pi a}}{2} cos(\theta/2)[\tau sin2\psi sin\theta + \frac{2}{3}(\sigma + \tau cos2\psi)cos^2(\theta/2)] \quad (14)$$

Maximizing K_I with respect θ gives,

$$\sigma_{xx} tan\left(\frac{\theta}{2}\right) + 2tan^2\left(\frac{\theta}{2}\right)\sigma_{xy} - \sigma_{xy} = 0 \quad (15)$$

Now again maximizing K_I with respect to 2ψ,

$$K_I = -\frac{3\sqrt{\pi a}}{2} cos(\theta/2)[\tau sin2\psi sin\theta + \frac{2}{3}(\sigma + \tau cos2\psi)cos^2(\theta/2)]$$

It gives,

$$tan2\psi = 3tan(\theta/2) \quad (16)$$

3.6 Interaction of Wing Cracks

Brittle solids consist of inhomogeneities such as tiny voids, microcracks or weakly bonded particles these defects can serve as initiation points for new cracks when material is subjected to stress. If the solid is loaded anyone of these can act as nuclei for the formation of new cracks.

The range of possible nuclei is broad, yet their characteristics likely fall between two limiting cases: a spherical void and a sharp inclined crack. Both possibilities have been studied by ref. [16], in both cases criterion for crack initiation is described as,

$$\sigma_1 = c_1\sigma_3 - \sigma_0$$

For this case from ref. [16] the cracks initiate when,

$$\sigma_1 = \frac{(1+\mu^2)^{\frac{1}{2}}+\mu}{(1+\mu^2)^{\frac{1}{2}}-\mu}\sigma_3 - \frac{\sqrt{3}}{(1+\mu^2)^{\frac{1}{2}}-\mu}\frac{K_{IC}}{\sqrt{\pi a}}$$

For ease of computation, it is convenient to normalize the equations by $K_{IC}/\sqrt{\pi a}$,giving

$$S_1 = c_1 S_3 - S_0$$

where $S_1 = \frac{\sigma_1\sqrt{\pi a}}{K_{IC}}$, $S_3 = \frac{\sigma_3\sqrt{\pi a}}{K_{IC}}$

$c_1 = \frac{(1+\mu^2)^{\frac{1}{2}}+\mu}{(1+\mu^2)^{\frac{1}{2}}-\mu}$ & $S_0 = \frac{\sqrt{3}}{(1+\mu^2)^{\frac{1}{2}}-\mu}$

The objective is to create a damage mechanics of brittle solids that will allow for the operational definition of failure and the derivation of the stress-strain response for a material with a specific defect population and set of elastic properties under a specific stress condition. In the following, the model proposed by ref. [19] are summarized.

The initial crack's faces experience a normal stress of σ and a shear stress of τ due to the remote field σ_1 , σ_3. Each wing crack's mouth is wedged open by δ as the crack slides, which is resisted by the coefficient of friction μ . One way to conceptualize the wedging is as the result of forces acting at the crack's midpoint, F_3, parallel to X_3. The stresses τ and σ are provided by ref. [19]:

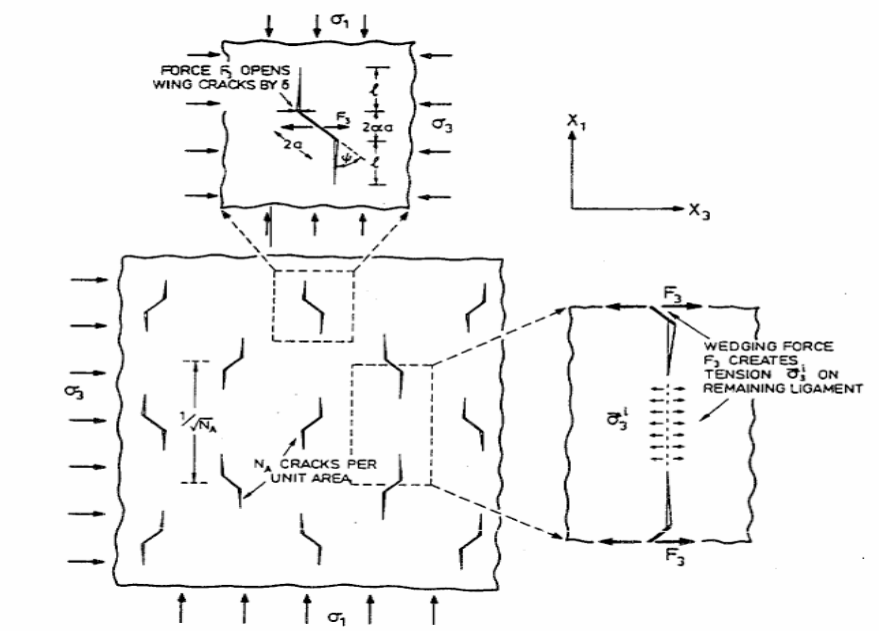

Fig. 3. 2: A population of growing wing cracks. Prior to incorporating the crack-crack interaction (illustrated on the right), we examine the growth of an isolated crack (shown above) (taken from ref. [19]).

$$\tau = \left(\frac{\sigma_3 - \sigma_1}{2}\right) sin2\psi$$
$$\sigma = \left(\frac{\sigma_3 + \sigma_1}{2}\right) + \left(\frac{\sigma_3 - \sigma_1}{2}\right) cos2\psi$$

F_3 is just the part of the sliding force that runs parallel to X_3 [19]:

$$F_3 = (\tau + \mu\sigma)2a \sin\psi$$

Or

$$F_3 = -(A_1\sigma_1 - A_3\sigma_3)a$$

When force F_3 is applied at the middle of a $2l$ crack, it produces a stress intensity that tends to open the crack [25]:

$$(K_I)_1 = \frac{F_3}{\sqrt{\pi l}}$$

When l is large, this result provides a good estimate of the stress intensity at the tip of a wing crack; however, when l is vanishingly small, it breaks down (becomes infinite). Although it is not infinite, the stress intensity at the initial inclined crack's tip can be precisely calculated using the formula from the previous section.

In order to resolve this issue, an "effective" crack length $(l + \beta a)$ is considered which provides [19]:

$$(K_I)_1 = \frac{F_3}{\sqrt{\pi(l+\beta a)}} \tag{17}$$

Following this, when l is zero, we select β so that $(K_I)_1$ equals that for the inclined crack [25]:

$$(K_I)_3 = \sigma_3\sqrt{\pi l} \tag{18}$$

Summing the two contributions with F_3 [19],

$$K_I = \frac{F_3}{\sqrt{\pi(l+\beta a)}} + \sigma_3\sqrt{\pi l}$$

$$K_I = -\frac{A_1\sigma_1\sqrt{\pi a}}{\pi\sqrt{L+\beta}} + \sigma_3\sqrt{\pi a}\left(\frac{A_3}{\pi\sqrt{L+\beta}} + L\right)$$

where $L = l/a$. The cracks extend until K_I becomes equal to K_{IC}

Making sure that this equation matches the known results for very long cracks $(L \gg 1)$ and reduces to the exact result for crack initiation $(L = 0)$ yields the constants [19]:

$$A_1 = \frac{\pi\sqrt{\beta}}{\sqrt{3}}\left[(1+\mu^2)^{\frac{1}{2}} - \mu\right]$$

$$A_3 = A_1 \left\{ \frac{(1+\mu^2)^{\frac{1}{2}}+\mu}{(1+\mu^2)^{\frac{1}{2}}-\mu} \right\}, \beta = 0.1 \tag{19}$$

The main part of figure shows an array of N_A cracks per unit area all of which have extended to length $2(L + \alpha a)$. The center to center spacing of the crack can be assumed to be [19],

$$S = \frac{1}{\sqrt{N_A}}$$

So that an uncracked ligament of average length $S - 2(L + \alpha a)$ remains between the cracks in X_1 direction. The average internal stress is given by [19],

$$\sigma_3^i = \frac{F_3}{S-2(L+\alpha a)} \tag{20}$$

This acts on the wing cracks, so that equation (18) becomes [19]:

$$(K_I)_3 = (\sigma_3 + \sigma_3^i)\sqrt{\pi l} \tag{21}$$

Defining the initial damage D_0 and current damage D states, as [19]:

$$D_0 = \pi(\alpha a)^2 N_A \tag{22a}$$
$$D = \pi(l + \alpha a)^2 N_A \tag{22b}$$

From Eqs. (20) and (22), the average internal stress can be expressed as [19]:

$$\sigma_3^i = \frac{-(A_1\sigma_1 - A_3\sigma_3)\left(\frac{D_0}{\pi}\right)^{\frac{1}{2}}}{\alpha\left(1-2\left(\frac{D}{\pi}\right)^{\frac{1}{2}}\right)} \tag{23}$$
$$K_I = \frac{F_3}{(\pi(l+\beta a))^{\frac{1}{2}}} + (\sigma_3 + \sigma_3^i)\sqrt{\pi l}$$

Substitution of Eqs. (23) and (17) into Eq. (21) gives [19]:

$$K_I = \frac{F_3}{\left(\pi(l + \beta a)\right)^{\frac{1}{2}}} + (\sigma_3 + \sigma_3^i)\sqrt{\pi l}$$
$$= \frac{-(A_1\sigma_1 - A_3\sigma_3)a}{\sqrt{\pi(l+\beta a)}} + \left(\sigma_3 - \frac{(A_1\sigma_1 - A_3\sigma_3)\left(\frac{D_0}{\pi}\right)^{\frac{1}{2}}}{\alpha\left(1-2\left(\frac{D}{\pi}\right)^{\frac{1}{2}}\right)} \right)$$

By using Eqs. 22(a) and (b), the relations between D and D_0 can be determined as [19]:

$$\left(\frac{D}{D_0}\right)^{\frac{1}{2}} - 1 = \frac{l+\alpha a}{\alpha a} - 1 = \frac{l}{\alpha a}$$

$$K_I = -\frac{A_1\sigma_1 a}{\sqrt{\pi(l+\beta a)}} + \frac{A_3\sigma_3 a}{\sqrt{\pi(l+\beta a)}} + \sigma_3\sqrt{\pi l} - \frac{A_1\sigma_1\left(\frac{D_0}{\pi}\right)^{\frac{1}{2}}}{\alpha\left(1-2\left(\frac{D}{\pi}\right)^{\frac{1}{2}}\right)}$$

$$+\frac{A_1\sigma_1\left(\frac{D_0}{\pi}\right)^{\frac{1}{2}}}{\alpha\left(1-2\left(\frac{D}{\pi}\right)^{\frac{1}{2}}\right)}$$

Now taking $A_1\sigma_1\sqrt{\pi a}$ common from all the terms will lead to expression,

$$= -A_1\sigma_1\sqrt{\pi a}\left[\frac{1}{\pi}\sqrt{\frac{a}{l+\beta a}} - \frac{A_3\sigma_3}{A_1\sigma_1}\frac{1}{\pi}\sqrt{\frac{a}{l+\beta a}} - \frac{\sigma_3}{\sigma_1 A_1}\sqrt{\frac{l}{a}} + \sqrt{\frac{l}{a}}\frac{\left(\frac{D_0}{\pi}\right)^{\frac{1}{2}}}{\alpha\left(1-2\left(\frac{D}{\pi}\right)^{\frac{1}{2}}\right)}\right.$$

$$\left. - \frac{A_3\sigma_3}{A_1\sigma_1}\sqrt{\frac{l}{a}}\frac{\left(\frac{D_0}{\pi}\right)^{\frac{1}{2}}}{\alpha\left(1-2\left(\frac{D}{\pi}\right)^{\frac{1}{2}}\right)}\right]$$

Also principal stress ratio $\lambda = \frac{\sigma_3}{\sigma_1}$,

$$\pi\sqrt{\frac{l+\beta a}{a}} = \pi\left(\frac{l+\beta a}{a}\right)^{\frac{1}{2}}$$

$$= \pi\left(\frac{l}{a}+\beta\right)^{\frac{1}{2}} = \pi\sqrt{\alpha}\left(\frac{l}{\alpha a}+\frac{\beta}{\alpha}\right)^{\frac{1}{2}}$$

$$= \pi\sqrt{\alpha}\left(\frac{l}{\alpha a}+1-1+\frac{\beta}{\alpha}\right)^{\frac{1}{2}} = \pi\sqrt{\alpha}\left(\frac{l+\alpha a}{\alpha a}-1+\frac{\beta}{\alpha}\right)^{\frac{1}{2}}$$

Thus,

$$\pi\sqrt{\alpha}\left(\frac{l+\alpha a}{\alpha a}-1+\frac{\beta}{\alpha}\right)^{\frac{1}{2}} = \pi\sqrt{\frac{l+\beta a}{a}}$$

$$= -\frac{A_1\sigma_1\sqrt{\pi a}}{\pi\sqrt{\frac{l+\beta a}{a}}}\left[1 - \frac{A_3\lambda}{A_1} - \frac{\lambda\pi}{A_1}\sqrt{\frac{l}{a}}\sqrt{\frac{l+\beta a}{a}} + \pi\sqrt{\frac{l}{a}}\sqrt{\frac{l+\beta a}{a}}\frac{\left(\frac{D_0}{\pi}\right)^{\frac{1}{2}}}{\alpha\left(1-2\left(\frac{D}{\pi}\right)^{\frac{1}{2}}\right)} - \frac{A_3\lambda\pi}{A_1}\sqrt{\frac{l+\beta a}{a}}\sqrt{\frac{l}{a}}\frac{\left(\frac{D_0}{\pi}\right)^{\frac{1}{2}}}{\alpha\left(1-2\left(\frac{D}{\pi}\right)^{\frac{1}{2}}\right)}\right]$$

$$= -\frac{A_1\sigma_1\sqrt{\pi a}}{\pi\sqrt{\frac{l+\beta a}{a}}}\left[\left(1-\frac{A_3\lambda}{A_1}\right) + \pi\sqrt{\frac{l+\beta a}{a}}\sqrt{\frac{l}{a}}\frac{\left(\frac{D_0}{\pi}\right)^{\frac{1}{2}}}{\alpha\left(1-2\left(\frac{D}{\pi}\right)^{\frac{1}{2}}\right)}\left(1-\frac{A_3\lambda}{A_1}\right) - \frac{\pi\lambda}{A_1}\sqrt{\frac{l+\beta a}{a}}\sqrt{\frac{l}{a}}\right]$$

$$= -\frac{A_1\sigma_1\sqrt{\pi a}}{\pi\sqrt{\frac{l+\beta a}{a}}}\left[\left(1-\frac{A_3\lambda}{A_1}\right)\left(1 + \pi\sqrt{\frac{l+\beta a}{a}}\sqrt{\frac{l}{a}}\frac{\left(\frac{D_0}{\pi}\right)^{\frac{1}{2}}}{\alpha\left(1-2\left(\frac{D}{\pi}\right)^{\frac{1}{2}}\right)}\right) - \frac{\pi\lambda}{A_1}\sqrt{\frac{l+\beta a}{a}}\sqrt{\frac{l}{a}}\right]$$

For $\beta \ll 1$,

$$= -\frac{A_1\sigma_1\sqrt{\pi a}}{\pi\sqrt{\frac{l+\beta a}{a}}}\left[\left(1-\frac{A_3\lambda}{A_1}\right)\left(1 + \frac{\pi l}{a}\frac{\left(\frac{D_0}{\pi}\right)^{\frac{1}{2}}}{\alpha\left(1-2\left(\frac{D}{\pi}\right)^{\frac{1}{2}}\right)}\right) - \frac{\pi\lambda}{A_1}\frac{l}{a}\right]$$

But $\frac{l}{a} = \left(\frac{D}{D_0}\right)^{\frac{1}{2}} - 1$

$$= -\frac{A_1\sigma_1\sqrt{\pi a}}{\pi\sqrt{\alpha}\left(\left(\frac{D}{D_0}\right)^{\frac{1}{2}} - 1 + \frac{\beta}{\alpha}\right)^{\frac{1}{2}}}\left[\left(1-\frac{A_3\lambda}{A_1}\right)\left(1 + \frac{\pi\left(\frac{D_0}{\pi}\right)^{\frac{1}{2}}\left(\left(\frac{D}{D_0}\right)^{\frac{1}{2}} - 1\right)}{\alpha\left(1-2\left(\frac{D}{\pi}\right)^{\frac{1}{2}}\right)}\right) - \frac{\pi\lambda}{A_1}\left(\left(\frac{D}{D_0}\right)^{\frac{1}{2}} - 1\right)\right]$$

The values of the constants are [19],

$$c_1 = \frac{A_3}{A_1} = \left\{\frac{(1+\mu^2)^{\frac{1}{2}}+\mu}{(1+\mu^2)^{\frac{1}{2}}-\mu}\right\}$$

$$c_2 = \frac{\pi\sqrt{\alpha}}{A_1} = \frac{\sqrt{\frac{3\alpha}{\beta}}}{(1+\mu^2)^{\frac{1}{2}} - \mu}\ , c_3 = \sqrt{\pi}$$

$$c_4 = \frac{\pi\alpha}{A_1} = \frac{\sqrt{\frac{3}{\beta}}}{(1+\mu^2)^{\frac{1}{2}}-\mu} \tag{24}$$

Also,

$$S_1 = c_1 S_3 - S_0 \ ,$$

$$S_1 = \frac{\sigma_1 \sqrt{\pi a}}{K_{IC}}$$

$$S_3 = \frac{\sigma_3 \sqrt{\pi a}}{K_{IC}}, S_0 = \frac{\sqrt{3}}{(1+\mu^2)^{\frac{1}{2}} - \mu}$$

$$S_1 = \frac{\sigma_1 \sqrt{\pi a}}{-\frac{A_1 \sigma_1 \sqrt{\pi a}}{\pi \sqrt{\alpha}\left(\left(\frac{D}{D_0}\right)^{\frac{1}{2}} - 1 + \frac{\beta}{\alpha}\right)^{\frac{1}{2}}} \left[\left(1 - \frac{A_3 \lambda}{A_1}\right)\left(1 + \frac{\pi\left(\frac{D_0}{\pi}\right)^{\frac{1}{2}}\left(\left(\frac{D}{D_0}\right)^{\frac{1}{2}} - 1\right)}{\alpha\left(1 - 2\left(\frac{D}{\pi}\right)^{\frac{1}{2}}\right)}\right) - \frac{\pi\lambda}{A_1}\left(\left(\frac{D}{D_0}\right)^{\frac{1}{2}} - 1\right)\right]}$$

$$= \frac{-\frac{\pi\sqrt{\alpha}}{A_1}\left(\left(\frac{D}{D_0}\right)^{\frac{1}{2}} - 1 + \frac{\beta}{\alpha}\right)^{\frac{1}{2}}}{(1 - c_1\lambda)\left[1 + \frac{c_3 D_0^{\frac{1}{2}}\left(\left(\frac{D}{D_0}\right)^{\frac{1}{2}} - 1\right)}{1 - D^{\frac{1}{2}}}\right] - c_4\lambda\left(\left(\frac{D}{D_0}\right)^{\frac{1}{2}} - 1\right)}$$

3.7 A micromechanics based Constitutive Model for failure at high strain rate

In this section, the model proposed by ref. [20] is presented. This model can be considered to be an extension of the theory proposed by ref. [19] and ref. [26] to accommodate the strain rate effects on brittle fracture of rocks and ceramics. This model have successfully shown predict the fracture behavior of Dionysus-Pentelicon marble under high strain rates.

In contrast to the model of ref. [26], the present model employs a dynamic crack growth law which is valid over a wide range of loading rates. Also, this model is more convenient to implement in the strain based finite element framework.

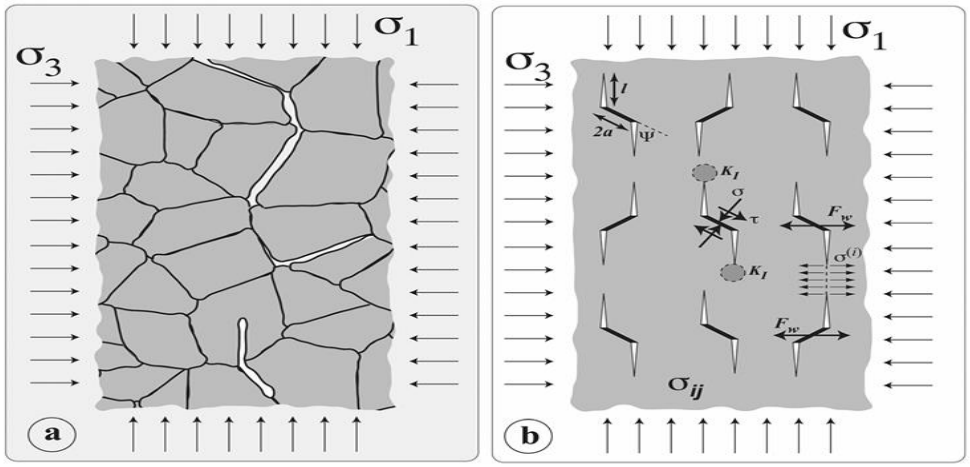

Fig. 3. 3 : Geometry of damage mechanics model (taken from ref. [20])

The key equations of the model are taken from ref. [20] and presented in the following, The stress-strain relationship and compliance tensor, M_{ijkl}, determined from Gibbs free energy function $W(\sigma, S)$as [20]:

$$\varepsilon_{ij} = \frac{\partial W(\sigma,S)}{\partial \sigma_{ij}} \ , \ M_{ijkl} = \frac{\partial^2 [W(\sigma,S)]}{\partial \sigma_{ij} \partial \sigma_{kl}}$$

Here dW denotes change in free energy function for solid undergoing change from state S to $S + dS$ at constant σ_{ij}. The expression for inelastic strain associated with dW is given by [20]:

$$d\varepsilon_{ij} = \frac{\partial (dW)}{\partial \sigma_{ij}}$$

Let Γ represent locus of all crack fronts in damaged solid & ds be a function of position along Γ describing local advance of microcracks, then change in free energy function is,

$$dW = \int_{\Gamma} \{[G(\sigma, S) - 2\gamma_s] ds\} d\Gamma$$

The inelastic strain is given by,

$$d\varepsilon_{ij} = \frac{\partial}{\partial \sigma_{ij}} \left[\int_{\Gamma} G(\sigma, S) ds d\Gamma \right] = \frac{\partial (\Delta W)}{\partial \sigma_{ij}}$$

The expression of energy release rate G related to stress intensity factor by,

$$G(\sigma, S) = \frac{1-\vartheta^2}{E} \left[K_I^2(\sigma, S) + K_{II}^2(\sigma, S) + \frac{K_{III}^2(\sigma,S)}{1-\vartheta} \right]$$

The above expression in valid for cracks without sudden kinks, forks & branches, thus by [20]:

$$\Delta W(\sigma, S) = \frac{1-\vartheta^2}{E} \int_{\Gamma} \left[K_I^2(\sigma, S) + K_{II}^2(\sigma, S) + \frac{K_{III}^2(\sigma,S)}{1-\vartheta} \right] ds \, d\Gamma$$

Gibbs free energy function is expressed as the summation of elastic and inelastic contributions, due to the presence of micro-cracks.

$$W(\sigma, S) = \mathrm{W}^{\mathrm{e}}(\sigma) + \frac{1-\vartheta^2}{E} \int_{\Gamma} \left[K_I^2(\sigma, S) + K_{II}^2(\sigma, S) + \frac{K_{III}^2(\sigma,S)}{1-\vartheta} \right] ds \, d\Gamma$$

From ref. [20], we categorize three deformation regimes for microcrack solid based on the applied loading state. In **Regime I**, the remote loading is compressive but insufficient to overcome the frictional resistance

on penny-shaped cracks, causing the solid to behave as an isotropic linear elastic material. In **Regime II**, the remote compressive load surpasses the frictional resistance, initiating the nucleation and growth of wing cracks from the micro-cracks.

In **Regime III**, the remote loading becomes tensile, resulting in the opening of both penny-shaped cracks and wing cracks. The criteria governing transitions between these regimes will be detailed later in the text.

$Regime\ II$: Following [19, 26] we evaluate Mode-I stress intensity factor(K_I) at the tip of the wing cracks. The Mode-I stress intensity factor, which drives crack growth in materials, comes from three main sources. First, when penny-shaped cracks slide under stress, they create a wedging force,F_w that pushes wing cracks open.

This force is the part of the sliding force aligned perpendicular to the maximum principal stress, calculated as $F_w = (\tau + f\sigma)\pi a^2\ sin\ \psi$, a is the crack radius, and ψ is the angle of the crack relative to the stress direction. Second, the remote compressive stress, denoted by σ , works to close the wing cracks, counteracting their opening.

Finally, the wedging force, F_w generates tensile stress σ^i, in the unbroken material between neighboring wing cracks, encouraging crack growth. Together, these factors shape how cracks propagate and affect the material's strength.

$$K_I^{R-II} = \frac{(\tau+f\sigma)\pi a^2 sin\psi}{[\pi(l+\beta a)]^{\frac{3}{2}}} + \frac{2}{\pi}(\sigma + \sigma^i)\sqrt{\pi l} \tag{25}$$

where $\sigma^i = \frac{(\tau+f\sigma)\pi a^2 sin\psi}{A_{crack}-\pi(l+\alpha a)^2}$; $A_{crack} = \pi^{\frac{1}{3}}\left(\frac{3}{4N_v}\right)^{\frac{2}{3}}$

We define a scalar damage parameter to represent both the current size of each crack and volume density of such cracks.

$$D = \frac{4}{3}\pi N_v(l + \alpha a)^3 \tag{26}$$

Rewriting eq. (25) in terms of D & D_0 we obtain,

$$K_I^{R-II}(\sigma, D) = \sqrt{\pi a}[A(D)\sigma + B(D)\tau] \tag{27}$$

$$A(D) = fc_1(D) + (1 + f)c_2(D)c_3(D)$$

$$B(D) = c_1(D) + c_2(D)c_3(D)$$

And

$$c_1(D) = \frac{\sqrt{1-\alpha^2}}{\pi\alpha^{\frac{3}{2}}\left[\left(\frac{D}{D_o}\right)^{\frac{1}{3}}-1+\frac{\beta}{\alpha}\right]^{\frac{3}{2}}},\ c_2(D) = \left(\frac{\sqrt{1-\alpha^2}}{\alpha}\right)\left(\frac{D_0^{\frac{2}{3}}}{1-D^{\frac{2}{3}}}\right)$$

$$c_3(D) = \frac{2\sqrt{\alpha}}{\pi}\left[\left(\frac{D}{D_o}\right)^{\frac{1}{3}} - 1\right]^{\frac{1}{2}}$$

Regime III: From ref. [26] we allow the possibility of overall loading turning tensile. We write the Mode I stress intensity factor as quadratic function of stress [27,28,29]:

$$K_I^{R-III}(\sigma, D) = \sqrt{\pi a}[C^2(D)\sigma^2 + E^2(D)\tau^2] \tag{28}$$

In general, the calculations start with the evaluation of the Gibbs free energy function for Regime's I, II and III using the SIF's (stress intensity factors) that we have calculated in the previous section,

- $Regime\ I$: For this regime the stress-strain relationship can be described as below,

$$\sigma_{ij} = 2\mu\varepsilon_{ij} + \frac{2\mu\vartheta}{1-2\vartheta}\varepsilon\delta_{ij} \tag{29}$$

- $Regime\ II$: The Gibbs free energy function can be written as,

$$W(\sigma, D) = W^e(\sigma) + \frac{1}{4\mu}[A_1\sigma + B_1\tau]^2$$

where $\tau = \sqrt{\frac{1}{2}S_{ij}S_{ij}}$ and $\sigma = \frac{\sigma_{kk}}{3}$, $S_{ij} = \sigma_{ij} - \sigma\,\delta_{ij}$,

$$W^e(\sigma) = \frac{1}{2}\sigma_{ij}\varepsilon_{ij}$$

$$W = \frac{1}{2}\sigma_{ij}\varepsilon_{ij} + \frac{1}{4\mu}\left[\frac{A_1\sigma_{kk}}{3} + B_1\tau\right]^2$$

$$\tau = \sqrt{\frac{1}{2}S_{ij}S_{ij}} = \sqrt{\frac{1}{2}(\sigma_{ij} - \frac{\sigma_{kk}}{3}\delta_{ij})(\sigma_{ij} - \frac{\sigma_{kk}}{3}\delta_{ij})}$$

$$= \sqrt{\frac{1}{2}\left(\sigma_{ij}.\sigma_{ij} - \frac{\sigma_{ij}.\sigma_{kk}\delta_{ij}}{3} - \frac{\sigma_{ij}.\sigma_{kk}\delta_{ij}}{3} + \frac{\sigma_{kk}\sigma_{mm}\delta_{ij}\delta_{ij}}{9}\right)}$$

$$\tau = \sqrt{\frac{1}{2}\left(\sigma_{ij}\sigma_{ij} - \frac{\sigma_{kk}\sigma_{mm}}{3}\right)}$$

$$W = \frac{1}{2}\sigma_{ij}\varepsilon_{ij} + \frac{1}{4\mu}\underbrace{\left[\frac{A_1\sigma_{kk}}{3} + B_1\tau\right]}_{x}^2$$

Now we will differentiate the above expression w.r.t stress to obtain the stress-strain relation,

$$\frac{\partial W}{\partial \sigma_{ml}} = \frac{1}{2}\frac{\partial \sigma_{ij}}{\partial \sigma_{ml}}\varepsilon_{ij} + \frac{1}{2}\sigma_{ij}\frac{\partial \varepsilon_{ij}}{\partial \sigma_{ml}} + \frac{1}{4\mu}\left[2x\ \frac{\partial}{\partial \sigma_{ml}}\left(\frac{A_1\sigma_{kk}}{3} + B_1\left(\sqrt{\frac{1}{2}\left(\sigma_{ij}\sigma_{ij} - \frac{\sigma_{kk}\sigma_{pp}}{3}\right)}\right)\right)\right]$$

Let $y = \frac{1}{2}\left(\sigma_{ij}\sigma_{ij} - \frac{\sigma_{kk}\sigma_{mm}}{3}\right)$

$$\frac{\partial W}{\partial \sigma_{ml}} = \varepsilon_{ml} + \frac{1}{4\mu}\left[2x\left(\frac{A_1\delta_{km}\delta_{kl}}{3} + \frac{B_1}{2\sqrt{y}}\frac{1}{2}\left(2\sigma_{ml} - \frac{\sigma_{pp}}{3}\delta_{km}\delta_{kl} - \frac{\sigma_{kk}}{3}\delta_{pm}\delta_{pl}\right)\right)\right]$$

$$= \varepsilon_{ml} + \frac{1}{4\mu}\left[2x\ \left(\frac{A_1\delta_{ml}}{3} + \frac{B_1}{2\sqrt{y}}\sigma_{ml} - \frac{B_1\sigma_{pp}\delta_{ml}}{6\sqrt{y}}\right)\right]$$

Substituting $x = \frac{A_1\sigma_{kk}}{3} + B_1\tau$,

$$= \varepsilon_{ml} + \frac{1}{4\mu}\left[2\left(\frac{A_1\sigma_{kk}}{3} + B_1\tau\right)\left(\frac{A_1}{3}\delta_{ml} + \frac{B_1\sigma_{ml}}{2\sqrt{y}} - \frac{B_1\sigma_{pp}\delta_{ml}}{6\sqrt{y}}\right)\right]$$

Apparently, we are aware $\sqrt{y} = \tau$ and rearranging the terms,

$$= \varepsilon_{ml} + \frac{1}{4\mu}\left[\frac{2}{9}A_1^2\sigma_{kk}\delta_{ml} + \frac{A_1B_1\sigma_{kk}\sigma_{ml}}{3\tau} - \frac{A_1B_1\sigma_{kk}\sigma_{pp}\delta_{ml}}{9\tau} + \frac{2}{3}A_1B_1\tau\delta_{ml} + B_1^2\sigma_{ml} - \frac{B_1^2}{3}\sigma_{mm}\delta_{ml}\right]$$

$$= \varepsilon_{ml} + \frac{1}{4\mu}\left[\frac{2}{3}A_1^2\sigma\delta_{ml} + \frac{A_1B_1\sigma\sigma_{ml}}{\tau} - \frac{A_1B_1\sigma^2\delta_{ml}}{\tau} + \frac{2}{3}A_1B_1\tau\delta_{ml} + B_1^2\sigma_{ml} - B_1^2\sigma\delta_{ml}\right] \qquad (30)$$

We know from eq. (29),

$$\sigma_{ij} = 2\mu\varepsilon_{ij} + \frac{2\mu\vartheta}{1-2\vartheta}\varepsilon\delta_{ij} \quad \& \quad e_{ij} = \varepsilon_{ij} - \frac{\varepsilon}{3}\ \delta_{ij}\ ; \epsilon = \epsilon_{kk}$$

Substituting the deviatoric stress tensor to obtain stress,

$$\sigma_{ij} = 2\mu\left[e_{ij} + \frac{\varepsilon\delta_{ij}}{3}\right] + \frac{2\mu\vartheta}{1-2\vartheta}\varepsilon\delta_{ij}$$

$$= 2\mu e_{ij} + \frac{2\mu}{3}\varepsilon\delta_{ij} + \frac{2\mu\vartheta}{1-2\vartheta}\varepsilon\delta_{ij}$$

$$\sigma_{ij} = 2\mu e_{ij} + \frac{2\mu\varepsilon\delta_{ij}(1+\vartheta)}{3(1-2\vartheta)}$$

$$\sigma = \frac{\sigma_{kk}}{3} = \frac{1}{3}\left[2\mu e_{kk} + 2\mu\varepsilon\delta_{kk}\left(\frac{(1+\vartheta)}{3(1-2\vartheta)}\right)\right] = 2\mu\varepsilon\left(\frac{(1+\vartheta)}{3(1-2\vartheta)}\right) \qquad (31)$$

$$\varepsilon = \frac{3(1-2\vartheta)}{2\mu(1+\vartheta)}\ \sigma \qquad (32)$$

Substitution of ε from eq. (32) into Eq. (29) gives:

$$\sigma_{ij} = 2\mu\varepsilon_{ij} + \frac{2\mu\vartheta}{1-2\vartheta}\frac{3(1-2\vartheta)}{2\mu(1+\vartheta)}\,\sigma\delta_{ij} = 2\mu\varepsilon_{ij} + \frac{3\vartheta}{1+\vartheta}\sigma\delta_{ij}$$

$$2\mu\varepsilon_{ij} = \sigma_{ij} - \frac{3\vartheta}{1+\vartheta}\sigma\delta_{ij} \rightarrow\ \varepsilon_{ij} = \frac{1}{2\mu}\left\{\sigma_{ij} - \frac{3\vartheta}{1+\vartheta}\sigma\delta_{ij}\right\} \tag{33}$$

Substituting ε_{ij} from Eq. (33) into eq. (30),

$$\frac{\partial W}{\partial \sigma_{ml}} = \varepsilon_{ml} + \frac{1}{4\mu}\left[\frac{2}{3}A_1^2\sigma\delta_{ml} + \frac{A_1B_1\sigma\sigma_{ml}}{\tau} - \frac{A_1B_1\sigma^2\delta_{ml}}{\tau} + \frac{2}{3}A_1B_1\tau\delta_{ml} + B_1^2\sigma_{ml} - B_1^2\sigma\delta_{ml}\right]$$

$$= \frac{1}{2\mu}\left\{\sigma_{ml} - \frac{3\vartheta}{1+\vartheta}\sigma\delta_{ml}\right\} + \frac{1}{4\mu}\left[\frac{2}{3}A_1^2\sigma\delta_{ml} + \frac{A_1B_1\sigma\sigma_{ml}}{\tau} - \frac{A_1B_1\sigma^2\delta_{ml}}{\tau} + \frac{2}{3}A_1B_1\tau\delta_{ml} + B_1^2\sigma_{ml} - B_1^2\sigma\delta_{ml}\right]$$

On rearranging the terms, we get the final expression for strain in terms of stress,

$$\varepsilon_{ml} = \frac{1}{2\mu}\left\{\left(1 + \frac{A_1B_1\sigma}{2\tau} + \frac{B_1^2}{2}\right)\sigma_{ml} - \left(\frac{3\vartheta}{1+\vartheta} + \frac{A_1B_1\sigma}{2\tau} - \frac{A_1^2}{3} + \frac{B_1^2}{2}\right)\sigma\delta_{ml} + \left(\frac{A_1B_1}{3}\right)\tau\delta_{ml}\right\} \tag{34}$$

Following the same procedure & again differentiating the above expression w.r.t to stress to obtain compliance tensor,

$$M_{ijkl}(\sigma, D) = \frac{1}{2\mu}\left\{\begin{array}{c}\left(\frac{1}{2} + \frac{B_1^2}{2} + \frac{A_1B_1\sigma}{4\tau}\right)\left(\delta_{ki}\delta_{lj} + \delta_{li}\delta_{kj}\right) - \left(\frac{\vartheta}{1-\vartheta} + \frac{B_1^2}{6} - \frac{A_1^2}{9} + \frac{A_1B_1\sigma}{2\tau} + \frac{A_1B_1\sigma^3}{2\tau^3}\right)\delta_{ij}\delta_{kl} \\ + \left(\frac{A_1B_1}{6} + \frac{A_1B_1\sigma^2}{4\tau^2}\right)\left(\hat{\sigma}_{ij}\delta_{kl} + \delta_{ij}\hat{\sigma}_{kl}\right) - \left(\frac{A_1B_1\sigma}{4\tau}\right)\hat{\sigma}_{ij}\hat{\sigma}_{kl}\end{array}\right\} \tag{35}$$

In order to implement above constitutive model in strain based finite element program, the expression of stress should be in term of strains. Here we will recast Gibbs free energy function in terms of conjugate strains ε and γ , where

$$\sigma_{ij} = 2\mu\varepsilon_{ij} + \frac{2\mu\vartheta}{1-2\vartheta}\varepsilon\delta_{ij}$$

$$\sigma_{ij} = 2\mu\left[e_{ij} + \frac{\varepsilon\delta_{ij}}{3}\right] + \frac{2\mu\vartheta}{1-2\vartheta}\varepsilon\delta_{ij}$$

$$\sigma_{ij} = 2\mu e_{ij} + 2\mu\varepsilon\delta_{ij}\left(\frac{1+\vartheta}{3(1-2\vartheta)}\right)$$

The elastic Gibb's free energy is given by,

$$W^e(\sigma) = \frac{1}{2}\sigma_{ij}\varepsilon_{ij}$$

$$= \frac{1}{2}\left(2\mu e_{ij} + 2\mu\varepsilon\delta_{ij}\left(\frac{1+\vartheta}{3(1-2\vartheta)}\right)\right)\left(e_{ij} + \frac{\varepsilon\delta_{ij}}{3}\right)$$

$$= \frac{1}{2}\left(2\mu e_{ij}e_{ij} + \frac{2}{3}\mu\varepsilon e_{ij}\delta_{ij} + 2\mu\varepsilon\delta_{ij}\left(\frac{1+\vartheta}{3(1-2\vartheta)}\right)e_{ij} + \frac{2\mu\varepsilon^2}{3}\left(\frac{1+\vartheta}{3(1-2\vartheta)}\right)\delta_{ij}\delta_{ij}\right)$$

$$= \frac{1}{2}\left[\mu\gamma^2 + \frac{2\mu\varepsilon}{3}e_{kk} + 2\mu\varepsilon\left(\frac{1+\vartheta}{3(1-2\vartheta)}\right)e_{kk} + \frac{2\mu\varepsilon^2}{3}\left(\frac{1+\vartheta}{3(1-2\vartheta)}\right)(3)\right]$$

$$= \frac{1}{2}\left[\mu\gamma^2 + \frac{2(1+\vartheta)}{3(1-2\vartheta)}\mu\varepsilon^2\right]$$

From eq. (32),

$$\sigma = 2\mu\varepsilon\left(\frac{(1+\vartheta)}{3(1-2\vartheta)}\right)$$

$$S_{ij} = \sigma_{ij} - \sigma\delta_{ij} = 2\mu e_{ij} + \frac{2(1+\vartheta)}{3(1-2\vartheta)}\mu\varepsilon\delta_{ij} - \frac{2\mu(1+\vartheta)}{3(1-2\vartheta)}\varepsilon\delta_{ij} = 2\mu e_{ij}$$

$$S_{ij} = 2\mu e_{ij}$$

$$S_{ij}.S_{ij} = 2\mu e_{ij}.2\mu e_{ij} = 4\mu^2 e_{ij}.e_{ij}$$

$$= 4\mu^2\left(\frac{\gamma^2}{2}\right) = 2\mu^2\gamma^2$$

$$\tau = \sqrt{\frac{1}{2}S_{ij}S_{ij}} = \sqrt{\frac{1}{2}(2\mu^2\gamma^2)} = \mu\gamma \qquad (36)$$

$$W(\sigma, D) = W^e(\sigma) + \frac{1}{4\mu}[A_1\sigma + B_1\tau\,]^2$$

$$= \frac{1}{2}\left[\mu\gamma^2 + \frac{2(1+\vartheta)}{3(1-2\vartheta)}\mu\varepsilon^2\right] + \frac{1}{4\mu}\left[A_1\frac{2(1+\vartheta)}{3(1-2\vartheta)}\mu\varepsilon + B_1\mu\gamma\right]^2$$

$$\varepsilon = \varepsilon_{kk}, \gamma = \sqrt{2e_{ij}.e_{ij}}$$

$$\frac{\partial\gamma}{\partial\varepsilon_{kl}} = \frac{1}{2\gamma}\frac{\partial}{\partial\varepsilon_{kl}}(2e_{ij}.e_{ij}) = \frac{1}{\gamma}\frac{\partial}{\partial\varepsilon_{kl}}(e_{ij}.e_{ij}) \qquad (37)$$

$$e_{ij} = \varepsilon_{ij} - \frac{\varepsilon\delta_{ij}}{3},$$

$$e_{ij}.e_{ij} = \left(\varepsilon_{ij} - \frac{\varepsilon_{kk}\delta_{ij}}{3}\right)\left(\varepsilon_{ij} - \frac{\varepsilon_{mm}\delta_{ij}}{3}\right)$$

$$= \varepsilon_{ij}.\varepsilon_{ij} - \frac{2}{3}\varepsilon_{kk}\varepsilon_{mm} + \frac{1}{3}\varepsilon_{kk}\varepsilon_{mm} = \varepsilon_{ij}.\varepsilon_{ij} - \frac{1}{3}\varepsilon_{kk}\varepsilon_{mm}$$

$$e_{ij}.e_{ij} = \varepsilon_{ij}.\varepsilon_{ij} - \frac{1}{3}\varepsilon_{kk}\varepsilon_{mm} \qquad (38)$$

From eq. (37),

$$\frac{\partial \gamma}{\partial \varepsilon_{kl}} = \frac{1}{\gamma}\frac{\partial}{\partial \varepsilon_{kl}}\left(e_{ij}.e_{ij}\right) = \frac{1}{\gamma}\frac{\partial}{\partial \varepsilon_{kl}}\left(\varepsilon_{ij}.\varepsilon_{ij} - \frac{1}{3}\varepsilon_{kk}\varepsilon_{mm}\right)$$

$$= \frac{1}{\gamma}\left(\varepsilon_{ij}\frac{\partial \varepsilon_{ij}}{\partial \varepsilon_{kl}} + \varepsilon_{ij}\frac{\partial \varepsilon_{ij}}{\partial \varepsilon_{kl}} - \frac{2}{3}\varepsilon_{pp}\ \frac{\partial \varepsilon_{mm}}{\partial \varepsilon_{kl}}\right)$$

$$= \frac{1}{\gamma}\left[2\varepsilon_{ij} \times \frac{1}{2}\left(\delta_{ik}\delta_{jl} + \ \delta_{il}\delta_{jk}\right) - \frac{2}{3}\varepsilon_{pp}\delta_{kl}\right] = \frac{1}{\gamma}\left[\left(\varepsilon_{kl} + \varepsilon_{lk}\right) - \frac{2}{3}\varepsilon_{pp}\delta_{kl}\right]$$

$$= \frac{2}{\gamma}\left[\varepsilon_{kl} - \frac{\varepsilon_{pp}\delta_{kl}}{3}\right] = \frac{2e_{kl}}{\gamma}$$

$$\frac{\partial \gamma}{\partial \varepsilon_{kl}} = \frac{2e_{kl}}{\gamma} \tag{39}$$

$$\frac{\partial \varepsilon}{\partial \varepsilon_{kl}} = \frac{\partial \varepsilon_{rr}}{\partial \varepsilon_{kl}} = \delta_{rk}\delta_{rl} = \delta_{kl}$$

The elastic part of the Gibbs free energy is given by,

$$W^e(\sigma, D) = \frac{1}{2}\left[\mu\gamma^2 + \frac{2(1+\vartheta)}{3(1-2\vartheta)}\mu\varepsilon^2\right]$$

$$\frac{\partial W^e}{\partial \varepsilon_{kl}} = \frac{1}{2}\left[\mu(2\gamma)\frac{\partial \gamma}{\partial \varepsilon_{kl}} + \frac{2(1+\vartheta)}{3(1-2\vartheta)}\ \mu(2\varepsilon_{rr})\frac{\partial \varepsilon_{rr}}{\partial \varepsilon_{kl}}\right]$$

$$= \frac{1}{2}\left[2\mu\gamma\left(\frac{2e_{kl}}{\gamma}\right) + \frac{2(1+\vartheta)}{3(1-2\vartheta)}\ \mu(2\varepsilon_{rr})\delta_{rk}\delta_{rl}\right] = 2\mu e_{kl} + \frac{2(1+\vartheta)}{3(1-2\vartheta)}\ \mu\varepsilon_{rr}\delta_{kl}$$

$$\frac{\partial W^e}{\partial \varepsilon_{kl}} = 2\mu e_{kl} + \frac{2(1+\vartheta)}{3(1-2\vartheta)}\ \mu\varepsilon_{rr}\delta_{kl}$$

$$\frac{\partial W^e}{\partial \varepsilon_{kl}} = 2\mu\left(\varepsilon_{kl} - \frac{\varepsilon_{pp}\delta_{kl}}{3}\right) + \frac{2(1+\vartheta)}{3(1-2\vartheta)}\ \mu\varepsilon_{rr}\delta_{kl}$$

$$\frac{\partial W^e}{\partial \varepsilon_{kl}} = 2\mu\varepsilon_{kl} - \frac{2\mu}{3}\varepsilon_{pp}\delta_{kl} + \frac{2(1+\vartheta)}{3(1-2\vartheta)}\ \mu\varepsilon_{rr}\delta_{kl} \tag{40}$$

Now for the inelastic part,

$$W^{ie}(\sigma, D) = \frac{1}{4\mu}\left[A_1\frac{2(1+\vartheta)}{3(1-2\vartheta)}\mu\varepsilon + B_1\mu\gamma\right]^2$$

$$= \frac{1}{4\mu}\left[A_1^2\left(\frac{4\mu^2(1+\vartheta)^2}{9(1-2\ \vartheta)^2}\right)\varepsilon^2 + B_1^2\mu^2\gamma^2 + 2A_1B_1\gamma\varepsilon\mu^2\frac{2(1+\vartheta)}{3(1-2\vartheta)}\right]$$

$$\frac{\partial W^{ie}}{\partial \varepsilon_{kl}} = \frac{1}{4\mu}\left[A_1^2\left(\frac{4\mu^2(1+\vartheta)^2}{9(1-2\ \vartheta)^2}\right)(2\varepsilon_{rr})\frac{\partial \varepsilon_{rr}}{\partial \varepsilon_{kl}} + B_1^2\mu^2(2\gamma)\left(\frac{2e_{kl}}{\gamma}\right) + A_1B_1\frac{4(1+\vartheta)}{3(1-2\vartheta)}\mu^2\gamma\frac{\partial \varepsilon_{rr}}{\partial \varepsilon_{kl}}\right.$$
$$\left. + A_1B_1\frac{4(1+\vartheta)}{3(1-2\vartheta)}\ \mu^2\varepsilon_{rr}\frac{\partial \gamma}{\partial \varepsilon_{kl}}\right]$$

$$= \frac{1}{4\mu}\left[A_1^2\frac{8\mu^2(1+\vartheta)^2}{9(1-2\vartheta)^2}\varepsilon_{rr}\delta_{kl} + A_1B_1\frac{4(1+\vartheta)}{3(1-2\vartheta)}\ \mu^2\left(\gamma\delta_{kl} + \frac{\varepsilon_{rr}(2e_{kl})}{3}\right) + \ B_1^2\mu^2(4e_{kl})\right]$$

$$\frac{\partial W^{ie}}{\partial \varepsilon_{kl}} = A_1^2\frac{2\mu(1+\vartheta)^2}{9(1-2\vartheta)^2}\ \varepsilon_{rr}\delta_{kl} + \mu B_1^2e_{kl} + A_1B_1\frac{\mu(1+\vartheta)}{3(1-2\vartheta)}\gamma\delta_{kl} + 2A_1B_1\frac{\mu(1+\vartheta)}{3(1-2\vartheta)}\varepsilon_{rr}\frac{e_{kl}}{\gamma}$$

where $e_{kl} = \varepsilon_{kl} - \frac{\varepsilon\delta_{kl}}{3}$

$$\frac{\partial W^{ie}}{\partial \varepsilon_{kl}} = A_1^2 \frac{2\mu(1+\vartheta)^2}{9(1-2\vartheta)^2}\, \varepsilon_{rr}\delta_{kl} + \mu B_1^2 \varepsilon_{kl} - \frac{\mu B_1^2}{3}\, \varepsilon_{qq}\delta_{kl} + A_1 B_1 \frac{\mu(1+\vartheta)}{3(1-2\vartheta)}\gamma\delta_{kl} + 2A_1 B_1 \frac{\mu(1+\vartheta)}{3(1-2\vartheta)}\, \frac{\varepsilon_{rr}\varepsilon_{kl}}{\gamma} - 2A_1 B_1 \frac{\mu(1+\vartheta)}{3(1-2\vartheta)} \frac{\varepsilon_{rr}\varepsilon_{mm}\delta_{kl}}{3\gamma} \quad (41)$$

Adding both the eq. (40), (41) & after rearranging the terms,

$$\sigma_{ij} = \frac{\partial W}{\partial \varepsilon_{kl}} = 2\mu\left[\left(1 + A_1 B_1 \frac{(1+\vartheta)}{3(1-2\vartheta)}\frac{\varepsilon}{\gamma} + \frac{B_1^2}{2}\right)\varepsilon_{kl} + \left(\frac{\vartheta}{1-2\vartheta} - \frac{(1+\vartheta)}{3(1-2\vartheta)}\frac{A_1 B_1 \varepsilon}{3\gamma} - \frac{B_1^2}{6} + \frac{(1+\vartheta)^2}{9(1-2\vartheta)^2}\, A_1^2\right)\varepsilon\delta_{kl} + \left(A_1 B_1 \frac{(1+\vartheta)}{6(1-2\vartheta)}\right)\gamma\delta_{kl}\right]$$

Expressing the above equation in terms of damage dependent constants,

$$\overline{A_1}(D) = \frac{1}{2}(A_1 a_1 + B_1 b_1), \overline{B_1}(D) = \frac{1}{2}(A_1 a_1 + B_1 b_2)$$

where,

$$a_1 = \frac{1}{\Gamma}\left(1 + \frac{B_1^2}{2}\right), b_1 = -\frac{1}{\Gamma}\left(\frac{A_1 B_1}{2}\right)$$

$$b_2 = \frac{1}{\Gamma}\left[\frac{A_1^2}{2} + \frac{3(1-2\vartheta)}{2(1+\vartheta)}\right], \Gamma = \left[\frac{3(1-2\vartheta)}{2(1+\vartheta)} + \frac{3(1-2\vartheta)}{4(1+\vartheta)} B_1^2 + \frac{A_1^2}{2}\right]$$

$$\sigma_{ij} = 2\mu\left\{\left(1 + \frac{2\overline{A_1}\,\overline{B_1}\varepsilon}{\gamma} + 2\overline{B_1}^2\right)\varepsilon_{ij} + \left(\frac{\vartheta}{1-2\vartheta} - \frac{2\overline{A_1}\,\overline{B_1}\varepsilon}{3\gamma} - \frac{2\overline{B_1}^2}{3} + \overline{A_1}^2\right)\varepsilon\delta_{ij} + \left(\overline{A_1}\,\overline{B_1}\right)\gamma\delta_{ij}\right\} \quad (42)$$

If we differentiate the above expression σ_{ij} w.r.t stress, we will end up getting the expression of modulus tensor as stated below,

$$C_{ijkl} = 2\mu\left\{\begin{array}{c}\left(\frac{1}{2} + \frac{\overline{B_1^2}}{2} + \frac{2\overline{A_1}\,\overline{B_1}\varepsilon}{\gamma}\right)\left(\delta_{ki}\delta_{lj} + \delta_{li}\delta_{kj}\right) + \left(\frac{\vartheta}{1-2\vartheta} - \frac{2\overline{B_1^2}}{3} + \overline{A_1^2} - \frac{2\overline{A_1}\,\overline{B_1}\varepsilon}{\gamma} - \frac{4\overline{A_1}\,\overline{B_1}\varepsilon^3}{9\gamma^3}\right)\delta_{ij}\delta_{kl} \\ + \left(\frac{2\overline{A_1}\,\overline{B_1}}{\gamma} + \frac{4\overline{A_1}\,\overline{B_1}\varepsilon^2}{3\gamma^2}\right)\left(\hat{\varepsilon}_{ij}\delta_{kl} + \delta_{ij}\hat{\varepsilon}_{kl}\right) - \left(\frac{4\overline{A_1}\,\overline{B_1}\varepsilon}{\gamma}\right)\hat{\varepsilon}_{ij}\hat{\varepsilon}_k\end{array}\right\} \quad (43)$$

where $\hat{\varepsilon}_{ij} = \frac{\varepsilon_{ij}}{\gamma}$

- *Regime III* : The expression for Gibbs free energy function in regime III can be written as,

$$W(\sigma, D) = W^e(\sigma) + \frac{1}{4\mu}[C_1^2\sigma^2 + E_1^2\tau^2]$$

$$\tau = \sqrt{\frac{1}{2}S_{ij}S_{ij}} \;\&\; \sigma = \frac{\sigma_{kk}}{3}\,, S_{ij} = \sigma_{ij} - \sigma\delta_{ij}$$

$$W^e(\sigma) = \frac{1}{2}\sigma_{ij}\varepsilon_{ij}$$

$$\frac{\partial W}{\partial \sigma_{kl}} = \frac{1}{2}\frac{\partial \sigma_{ij}}{\partial \sigma_{kl}}\varepsilon_{ij} + \frac{1}{2}\sigma_{ij}\frac{\partial \varepsilon_{ij}}{\partial \sigma_{kl}} + \frac{1}{4\mu}\frac{\partial}{\partial \sigma_{kl}}\left[C_1^2\left(\frac{\sigma_{mm}^2}{9}\right) + E_1^2\tau^2\right]$$

$$= \varepsilon_{ij} + \frac{1}{4\mu}\left[C_1^2\left(\frac{2\sigma_{mm}}{9}\right)\delta_{jk}\delta_{jl} + E_1^2(2\tau)\frac{\partial \tau}{\partial \sigma_{kl}}\right]$$

$$\frac{\partial \tau}{\partial \sigma_{kl}} = \frac{\partial}{\partial \sigma_{kl}}\left[\sqrt{\frac{1}{2}S_{ij}S_{ij}}\right] = \frac{1}{4\tau}\frac{\partial}{\partial \sigma_{kl}}\left[\sigma_{ij}\sigma_{ij} - \frac{\sigma_{mm}\sigma_{jj}}{3}\right]$$

$$= \frac{1}{4\tau}\left[(\sigma_{lk} + \sigma_{kl}) - \frac{2}{3}\sigma_{mm}\delta_{kl}\right] = \frac{1}{4\tau}[2(\sigma_{kl} - \sigma\delta_{kl})]$$

$$\frac{\partial \tau_{ij}}{\partial \sigma_{kl}} = \frac{1}{2\tau}\,S_{kl} \tag{44}$$

$$\frac{\partial W}{\partial \sigma_{kl}} = \varepsilon_{ij} + \frac{1}{4\mu}\left[C_1^2\left(\frac{2\sigma_{mm}}{9}\right)\delta_{jk}\delta_{jl} + E_1^2(2\tau_{ij})\frac{\partial \tau}{\partial \sigma_{kl}}\right]$$

Substituting value of ε_{ij} from eq. (33),

$$\frac{\partial W}{\partial \sigma_{kl}} = \frac{1}{2\mu}\left\{\sigma_{kl} - \frac{3\vartheta}{1+\vartheta}\sigma\delta_{kl}\right\} + \frac{1}{4\mu}\left\{C_1^2\left(\frac{2\sigma_{mm}}{9}\right)\delta_{kl} + E_1^2(2\tau)\frac{1}{2\tau}\,S_{kl}\right\}$$

$$= \frac{1}{2\mu}\left\{\sigma_{kl} - \frac{3\vartheta}{1+\vartheta}\sigma\delta_{kl} + \frac{C_1^2}{3}\sigma\delta_{kl} + \frac{E_1^2}{2}(\sigma_{kl} - \sigma\delta_{kl})\right\}$$

$$\frac{\partial W}{\partial \sigma_{kl}} = \varepsilon_{kl} = \frac{1}{2\mu}\left\{\left(1 + \frac{E_1^2}{2}\right)\sigma_{kl} - \left(\frac{3\vartheta}{1+\vartheta} + \frac{E_1^2}{2} - \frac{C_1^2}{3}\right)\sigma\delta_{kl}\right\} \tag{45}$$

Differentiating the above equation w.r.t stress we obtain the compliance tensor,

$$M_{ijkl}(\sigma, D) = \frac{1}{2\mu}\left\{\left(1 + \frac{E_1^2}{4}\right)(\delta_{ki}\delta_{lj} + \delta_{li}\delta_{kj}) - \left(\frac{\vartheta}{(1+\vartheta)} + \frac{E_1^2}{6} - \frac{C_1^2}{9}\right)\delta_{ij}\delta_{kl}\right\} \tag{46}$$

Here we will recast Gibbs free energy function in terms of conjugate strains ε and γ , where

$$W(\sigma, D) = W^e(\sigma) + \frac{1}{4\mu}[C_1^2\sigma^2 + E_1^2\tau^2\,]$$

$$= \frac{1}{2}\left[\mu\gamma^2 + \frac{2(1+\vartheta)}{3(1-2\vartheta)}\mu\varepsilon^2\right] + \frac{1}{4\mu}[C_1^2\sigma^2 + E_1^2\tau^2\,]$$

We know from eq. (32), (36) $\sigma = \frac{2(1+\vartheta)}{3(1-2\vartheta)}\mu\varepsilon$ & $\tau = \mu\gamma$,

$$W(\epsilon, D) = \frac{1}{2}\left[\mu\gamma^2 + \frac{2(1+\vartheta)}{3(1-2\vartheta)}\mu\varepsilon^2\right] + \frac{1}{4\mu}\left[C_1^2\,\frac{4(1+\vartheta)^2}{9(1-2\vartheta)^2}\,\mu^2\varepsilon^2 + E_1^2\,\mu^2\gamma^2\right]$$

From eq. (38)

$$\frac{\partial W^e}{\partial \varepsilon_{kl}} = 2\mu\varepsilon_{kl} - \frac{2\mu}{3}\varepsilon_{kk}\delta_{kl} + \frac{2(1+\vartheta)}{3(1-2\vartheta)}\,\mu\varepsilon_{rr}\delta_{kl}$$

$$\frac{\partial W^{ie}}{\partial \varepsilon_{kl}} = \frac{1}{4\mu}\left[C_1^2\,\frac{4(1+\vartheta)^2}{9(1-2\vartheta)^2}\,\mu^2(2\varepsilon)\frac{\partial \varepsilon}{\partial \varepsilon_{kl}} + E_1^2\,\mu^2(2\gamma)\frac{\partial \gamma}{\partial \varepsilon_{kl}}\right]$$

As we have previously derived the relations $\frac{\partial \varepsilon}{\partial \varepsilon_{kl}} = \delta_{kl}, \frac{\partial \gamma}{\partial \varepsilon_{kl}} = \frac{2e_{kl}}{\gamma}$

$$= \frac{1}{4\mu}\left[C_1^2\,\frac{8(1+\vartheta)^2}{9(1-2\vartheta)^2}\,\mu^2\varepsilon\delta_{kl} + 2E_1^2\mu^2\gamma\left(\frac{2e_{kl}}{\gamma}\right)\right]$$

$$= \left[C_1^2\,\frac{2(1+\vartheta)^2}{9(1-2\vartheta)^2}\mu\varepsilon\delta_{kl} + E_1^2\mu\left(\varepsilon_{kl} - \frac{\varepsilon\delta_{kl}}{3}\right)\right]$$

$$\frac{\partial W^{ie}}{\partial \varepsilon_{kl}} = C_1^2\,\frac{2(1+\vartheta)^2}{9(1-2\vartheta)^2}\mu\varepsilon\delta_{kl} + E_1^2\mu\varepsilon_{kl} - \frac{E_1^2}{3}\mu\varepsilon\delta_{kl} \tag{47}$$

Adding both elastic & inelastic parts and after rearranging the terms,

$$\frac{\partial W}{\partial \varepsilon_{kl}} = \left[2\mu\varepsilon_{kl} - \frac{2\mu}{3}\varepsilon\delta_{kl} + \frac{2(1+\vartheta)}{3(1-2\vartheta)}\mu\varepsilon\delta_{kl} + C_1^2\,\frac{2(1+\vartheta)^2}{9(1-2\vartheta)^2}\mu\varepsilon\delta_{kl} + E_1^2\mu\varepsilon_{kl} - \frac{E_1^2}{3}\mu\varepsilon\delta_{kl}\right]$$

$$\sigma_{ij} = \frac{\partial W}{\partial \varepsilon_{kl}} = 2\mu\left[\left(1 + \frac{E_1^2}{2}\right)\varepsilon_{kl} + \left(\frac{\vartheta}{1-2\vartheta} - \frac{E_1^2}{6} + C_1^2\,\frac{(1+\vartheta)^2}{9(1-2\vartheta)^2}\right)\varepsilon\delta_{kl}\right] \tag{48}$$

Representing the above equations in terms of damage dependent constants $\overline{C_1}$ & $\overline{E_1}$,

$$\overline{C_1} = \frac{C_1}{\left\{\frac{3(1-2\vartheta)}{1+\vartheta} + C_1^2\right\}}, \overline{E_1} = \frac{E_1}{\left\{2 + E_1^2\right\}}$$

$$\sigma_{ij} = 2\mu\left[\left(1 + 2\,\overline{E_1}^2\right)\varepsilon_{kl} + \left(\frac{\vartheta}{1-2\vartheta} - \frac{2\,\overline{E_1}^2}{3} + \overline{C_1}^2\right)\varepsilon\delta_{kl}\right] \tag{49}$$

Again, differentiating the above expression to obtain the modulus tensor,

$$C_{ijkl} = 2\mu\left\{\left(\frac{1}{2} + \overline{E_1}^2\right)\left(\delta_{ki}\delta_{lj} + \delta_{li}\delta_{kj}\right) + \left(\frac{\vartheta}{1-2\vartheta} - \frac{2\,\overline{E_1}^2}{3} + \overline{C_1}^2\right)\delta_{ij}\delta_{kl}\right\} \tag{50}$$

Criterion of transition between regimes,

For $Regime\ I$

$$A\sigma + B\tau \leq 0 \tag{51}$$

The above condition suggests that the combined effect of stress related terms (σ, τ) & material parameters (A, B) does not exceed the threshold required for microcrack activation.

Transition from $Regime\ II$ to $Regime\ III$

In $Regime\ II$,

$$A\sigma + B\tau > 0 \quad \text{and} \quad (A^2 - C^2)\sigma + AB\tau > 0 \tag{52}$$

The transition to Regime II occurs when stresses increase enough to initiate microcrack sliding or partial activation, as indicated above.

In $Regime\ III$,

$$A\sigma + B\tau > 0 \quad \text{and} \quad (A^2 - C^2)\sigma + AB\tau < 0 \tag{53}$$

In Regime III, the stresses are high enough to cause significant microcrack opening or extensive sliding, the remote loading turns tensile which leads to opening of both wing & penny shaped cracks as both conditions are satisfied

The most important part of model i.e., rate dependent fracture toughness is not discussed. It should be discussed here because this is the most important extension in model and you have also used in the next chapter.

3.8 Evolution Law for Damage (D)

To complete the constitutive model discussed above, a particular evolution law for the scalar damage parameter D, is to be implemented. Differentiating D (eq.26) with respect to time, we obtain the rate of damage evolution.

The formulation allows the model to consider the time-dependent development of damage in ceramics under compressive stress, which corresponds to the effect of crack propagation and degradation of materials [20].

$$\frac{dD}{dt} = \left(\frac{3D^{\frac{2}{3}}D_0^{\frac{1}{3}}}{\alpha a}\right)\left(\frac{dl}{dt}\right) \tag{54}$$

where $\frac{dl}{dt} = v$ is instantaneous wing crack tip speed.

To address this problem effectively, it is crucial to analyse the stress state surrounding to the crack tip, both when stationary and during propagation, under diverse loading conditions. These stress values must then be compared with the experimentally measured fracture toughness of the material under comparable conditions to establish criteria for crack initiation and growth. Typically, such criteria stipulate that crack propagation occurs in a manner that maintains a material-specific parameter, such as the dynamic stress intensity factor (K_{IC}^{d}), at a constant value characteristic of the material.

Based on the experimental observations of ref. [20] we can now formulate an expression that captures both the initiation and growth of fractures under high loading rates.

- $Initiation\ Criterion$: The crack will initiate motion when [20],

$$K_I^d(v = 0, \dot{K}_I) = K_{IC}^d(\dot{K}_I) \tag{55}$$

where $K_{IC}^d = \left(1 + \left(\frac{\dot{K}_I}{K_{IC}^{SS}}\right) * 2 * 10^{-5}\right) * K_{IC}^{SS}$

$\dot{K}_I = \frac{K_{IC}}{t_c}$, K_{IC} = Mode I critical SIF at instant of crack initiation

K_I^d = Dynamic stress intensity factor

K_{IC}^{SS} = Quasi static stress intensity factor

- $Growth\ Criterion$: The dynamic stress intensity factor for the propagating crack is given by [20],

$$\frac{K_I(1-v/c_R)}{\sqrt{1-v/c_p}} = K_{IC}^{SS}\left\{\frac{1+\left(\frac{v}{v_m}\right)^5}{\sqrt{1-v/c_p}}\right\} \tag{56}$$

where v_m = Branching speed, v = Crack tip speed

c_p =Dilatational or P-wave speed, c_R = Rayleigh wave speed [46].

In the above equation K_I can be obtained from eq. (27) or (28) depending upon the loading regime. This expression is evaluated to determine the crack propagation speed(v), which is subsequently incorporated into Equation (54) to finalize the damage evolution equation.

Chapter 4

Numerical Implementation of Damage Model for Ceramics

4.1 Numerical Implementation

In this chapter, numerical implementation of fracture mechanics-based damage model proposed by ref. [20] has been presented. First of all, we would like to implement our damage constitutive model in MATLAB program. The flow chart explaining the algorithm employed in the implementation of model is presented in Fig. 4.1.

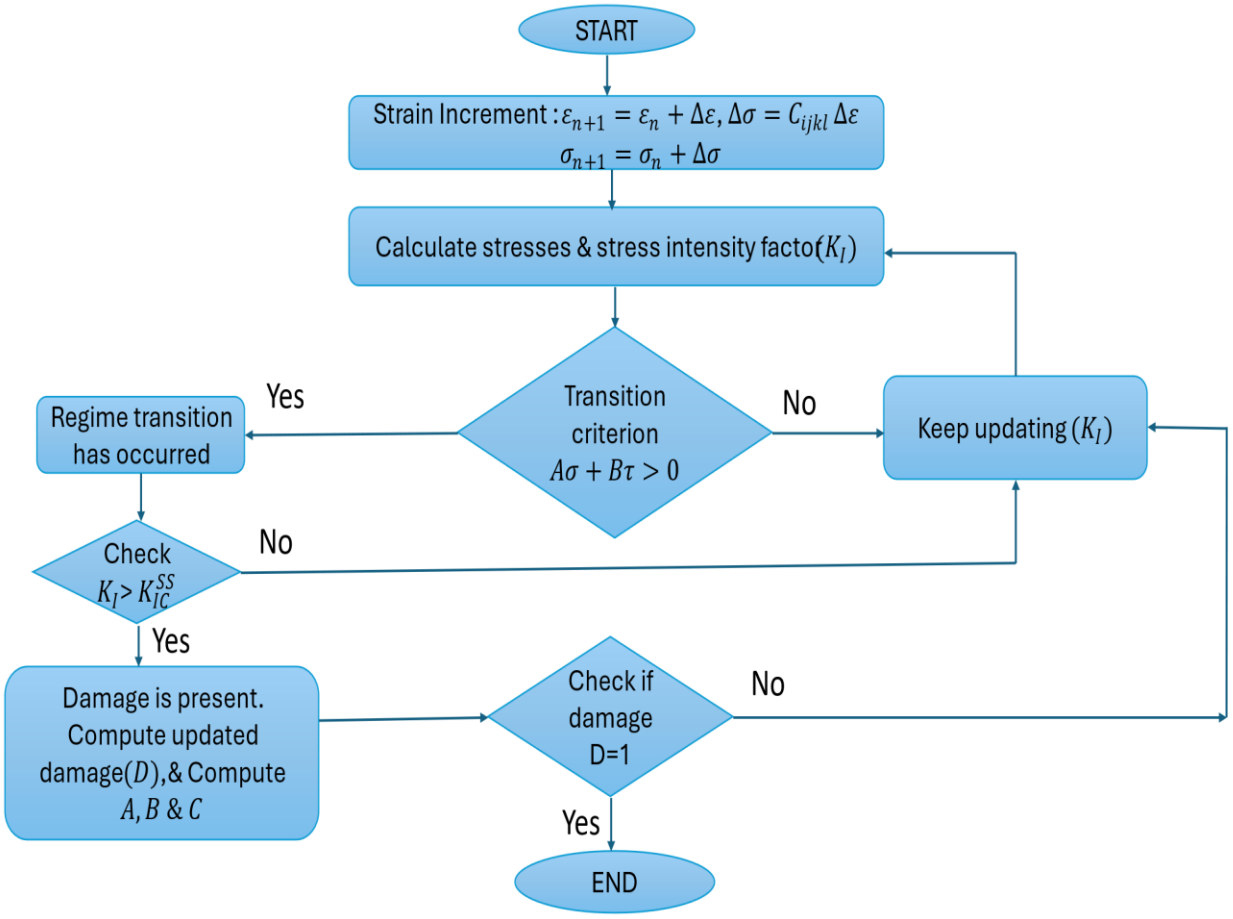

Fig. 4. 1 Algorithm diagram for implementing MATLAB program

In a uniaxial compression loading, where compressive stress is applied along a single axis while the other two axes are constrained (e.g., preventing lateral expansion), the mechanical behaviour of the material can be analyzed using a stress-strain graph. This graph serves as a critical tool for identifying the operational regime of the material under load.

Initially, as compression begins, the material operates in Regime I, known as the undamaged elastic regime. In this regime, the material exhibits linear elastic behaviour, where stress is proportional to strain according to Hooke's Law, and no permanent damage (e.g., micro-cracking or plastic deformation) occurs. As compressive stress increases, the material may transition from Regime I to a different regime, such as a damaged or plastic regime, depending on the material properties and loading conditions.

This transition is governed by a specific failure or yield criterion, expressed as $A\sigma + B\tau > 0$. This criterion indicates the onset of damage or a change in mechanical behaviour, such as the formation of micro-cracks, yielding, or other forms of inelastic deformation.

In the current case, the condition $A\sigma + B\tau > 0$ is not satisfied, implying that the applied stress remains below the threshold required for regime transition. Consequently, the material continues to operate within Regime I, maintaining its elastic and undamaged state.

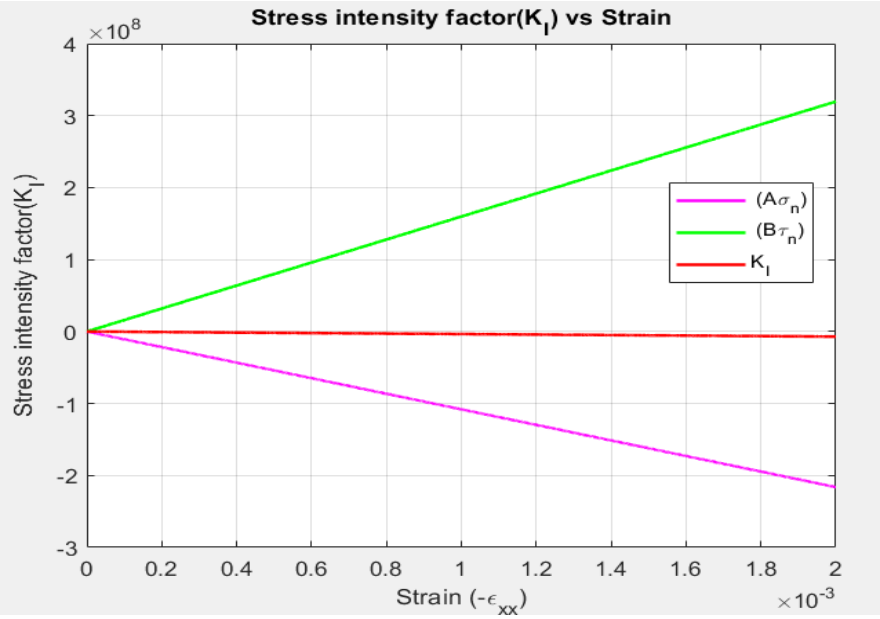

Fig. 4. 2 The variation of stress intensity factor, K_I with the applied normal strain, ϵ_{xx} along X axis for uniaxial compression loading.

Hydrostatic compression applies equal compressive forces to a material from all directions which produces a stress condition with equal principal stresses ($\sigma_1 = \sigma_2 = \sigma_3 = -\sigma$, where σ represents the compressive stress magnitude). The uniform stress distribution reduces shear stresses because no differential stresses create deviatoric deformation. The necessary factors to start damage processes including micro-crack initiation and crack extension and crack plane sliding are absent. The uniform stress conditions of hydrostatic compression lead to volume reduction without causing the stress concentrations which typically result in inelastic responses or material failure.

The material shows a complete elastic response without any damage which corresponds to Regime I of a damage model known as the intact or undamaged elastic regime. The material follows Hooke's Law in this regime by demonstrating a direct proportional connection between stress and strain while showing complete elastic deformation without any structural damage.

Hydrostatic compression produces a stress-strain behavior which depends on the bulk modulus to determine how resistant the material is to uniform compression. Since the hydrostatic stress state does not satisfy typical damage onset criteria (e.g., a critical stress threshold involving shear or tensile components, such as $A\sigma + B\tau > 0$ in other loading scenarios), the material remains in Regime I, with no transition to subsequent regimes associated with damage accumulation.

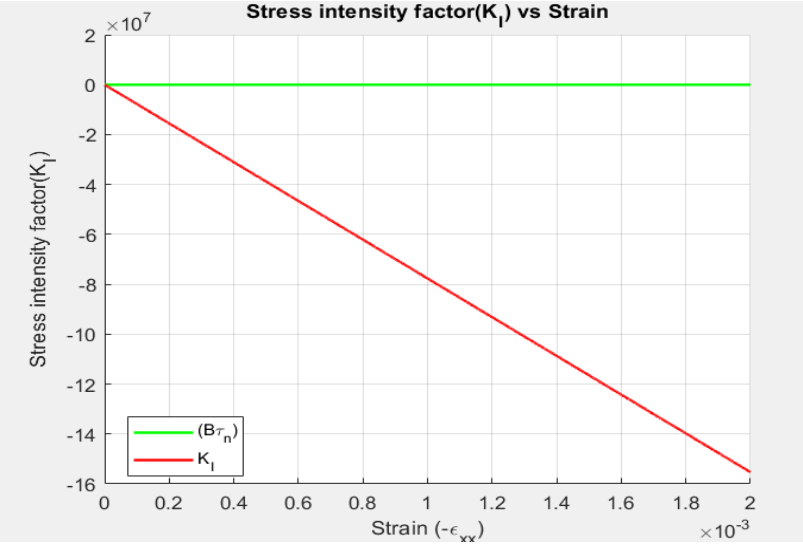

Fig. 4. 3:The variation of stress intensity factor K_I with applied normal strain ϵ_{xx} plot along X axis for hydrostatic compression loading.

The research excludes factors such as temperature variations and material heterogeneity which have the potential to affect stress distribution and transitions between different regimes.

Future scope of the project includes understanding regime transition criterions to predict the material failure behavior and to perform dynamic loading experiments (e.g., split Hopkinson pressure bar tests) to validate models under high strain rates.

REFERENCES

[1] Krajcinovic, Dusan, and Jean Lemaitre, eds. *Continuum damage mechanics: theory and applications*. New York: Springer-Verlag, 1987.

[2] Kachanov, Lasar. *Introduction to continuum damage mechanics*. Vol. 10. Springer Science & Business Media, 2013.

[3] Edrisi, Siroos, Norollah Kasiri Bidhendi, and Maryam Haghighi. "A new approach to modeling the effective thermal conductivity of ceramics porous media using a generalized self-consistent method." *Heat and Mass Transfer* 53 (2017): 321-330.

[4] Benloulo, IS Chocron, and V. Sanchez-Galvez. "A new analytical model to simulate impact onto ceramic/composite armors." *International journal of impact engineering* 21.6 (1998): 461-471.

[5] Imani, S. Misagh, et al. "The modified Mori-Tanaka scheme for the prediction of the effective elastic properties of highly porous ceramics." *Ceramics International* 44.14 (2018): 16489-16497.

[6] Benloulo, IS Chocron, and V. Sanchez-Galvez. "A new analytical model to simulate impact onto ceramic/composite armors." *International journal of impact engineering* 21.6 (1998): 461-471.

[7] Roberts, Anthony P., and Edward J. Garboczi. "Elastic properties of model porous ceramics." *Journal of the American Ceramic Society* 83.12 (2000): 3041-3048.

[8] Ravichandran, G. B. A. C. I. O. T., and G. B. A. C. I. O. T. Subhash. "A micromechanical model for high strain rate behavior of ceramics." *International Journal of Solids and structures* 32.17-18 (1995): 2627-2646.

[9] Tsukrov, Igor, and Jindrich Novak. "Effective elastic properties of solids with two-dimensional inclusions of irregular shapes." *International Journal of Solids and Structures* 41.24-25 (2004): 6905-6924.

[10] Petkovski, Mihail. "Experimental detection of damage evolution in concrete under multiaxial compression." *Journal of Engineering Mechanics* 139.5 (2013): 616-628.

[11] Zhao, L. Y., et al. "A unified micromechanics-based damage model for instantaneous and time-dependent behaviors of brittle rocks." *International Journal of Rock Mechanics and Mining Sciences* 84 (2016): 187-196.

[12] Yang, Qiang, Xin Chen, and Wei-Yuan Zhou. "On microscopic thermodynamic mechanisms of damage evolution laws." *International Journal of Damage Mechanics* 14.3 (2005): 261-293.

[13] Lajtai, E. Z. "A theoretical and experimental evaluation of the Griffith theory of brittle fracture." *Tectonophysics* 11.2 (1971): 129-156.

[14] Irwin, G. R. "Linear fracture mechanics, fracture transition, and fracture control." *Engineering fracture mechanics* 1.2 (1968): 241-257.

[15] Dong, Xiangyang, and Yung C. Shin. "Multiscale modeling for predicting the mechanical properties of silicon carbide ceramics." *Journal of the American Ceramic Society* 99.3 (2016): 1006-1014.

[16] M.F. Ashby, S.D. Hallam (Née Cooksley), The failure of brittle solids containing small cracks under compressive stress states, Acta Metallurgica, Volume 34, Issue 3, 1986, Pages 497-510, ISSN 0001-6160.

[17] Brace WF, Bombolakis EG. A note on brittle crack growth in compression. Journal of Geophysical Research. 1963 Jun 15;68(12):3709-13.

[18] Voyiadjis, G.Z., Zhou, Y. (2022). Frictional Contact Between a Blunt Tool and Quasi-brittle Rock with Damage: Numerical Modeling. In: Voyiadjis, G.Z. (eds) Handbook of Damage Mechanics. Springer, Cham.

[19] Ashby, M.F., Sammis, C.G. The damage mechanics of brittle solids in compression. *PAGEOPH* **133**, 489–521 (1990).

[20] Bhat, Harsha S., Ares J. Rosakis, and Charles G. Sammis. 2012. “A Micromechanics Based Constitutive Model for Brittle Failure at High Strain Rates”. Journal of Applied Mechanics 79 (3): Art. No. 031016.

[21] Introduction to Continuum Mechanics by C. Hartsuijker & J.W. Welleman iii November 2009.

[22] Diego J. Celentano, Jean-Louis Chaboche, Experimental and numerical characterization of damage evolution in steels, International Journal of Plasticity, Volume 23, Issues 10–11,2007,Pages 1739-1762,ISSN 0749-6419, https://doi.org/10.1016/j.ijplas.2007.03.008.

[23] Cotterell, Brian, and JRf Rice. "Slightly curved or kinked cracks." *International journal of fracture* 16 (1980): 155-169.

[24] Williams, Max L. "On the stress distribution at the base of a stationary crack." (1957): 109-114.

[25] Tada, Hiroshi, Paul C. Paris, and George R. Irwin. "The stress analysis of cracks." *Handbook, Del Research Corporation* 34.1973 (1973).

[26] Deshpande, V. S., and Evans, A. G., 2008, “Inelastic Deformation and Energy Dissipation in Ceramics: A Mechanism-Based Constitutive Model,” J. Mech. Phys. Solids, 56(10), pp. 3077–3100.

[27] Budiansky, B., and O’Connell, R. J., 1976, “Elastic Moduli of a Cracked Solid,” Int. J. Solids Struct., 12(2), pp. 81–97.

[28] Kachanov, M. L., 1987, “Elastic Solids with Many Cracks: A Simple Method of Analysis,” Int. J. Solids Struct., 23(1), pp. 23–43.

[29] Bristow, J. R., 1960, “Micro-Cracks, and the Static and Dynamic Elastic Constants of Annealed and Heavily Cold-Worked Metals,” Br. J. Appl. Phys., 11, pp. 81–85.

[30] Haberman, Keith Scott. *A micromechanical constitutive model for the dynamic response of brittle materials" Dynamic response of marble"*. Diss. California Institute of Technology, 2000.

[31] Barber, D.J., Meredith, P.G., Hallam, S.D. and Ashby, M.F., 1990. Compressive brittle fracture and the construction of multi-axial failure maps. *Deformation processes in minerals, ceramics and rocks*, pp.84-108.

[32] Brace, W.F. and Bombolakis, E.G., 1963. A note on brittle crack growth in compression. *Journal of Geophysical Research*, *68*(12), pp.3709-3713.

[33] Rosakis, A.J., Samudrala, O. and Coker, D., 1999. Cracks faster than the shear wave speed. *Science*, *284*(5418), pp.1337-1340.

[34] Chen, W., Song, B., Chen, W.W. and Song, B., 2011. Conventional kolsky bars. *Split Hopkinson (Kolsky) Bar: Design, Testing and Applications*, pp.1-35.

[35] Gray III, G.T., 2000. Classic split-Hopkinson pressure bar testing. In *Mechanical testing and evaluation* (pp. 462-476). ASM International.

[36] Kolsky, H., 1964. Stress waves in solids. *Journal of sound and Vibration*, *1*(1), pp.88-110.

[37] Lindholm, U.S. and Yeakley, L.M., 1968. High strain-rate testing: Tension and compression: In this paper, the authors present a split-pressure-bar method for obtaining complete stress-strain curves at strain rates in the order of 1000 sec− 1 in either tension or compression. *Experimental Mechanics*, *8*(1), pp.1-9.

[38] Nemat-Nasser, S., 2000. A micromechanically-based constitutive model for frictional deformation of granular materials. *Journal of the Mechanics and Physics of Solids*, *48*(6-7), pp.1541-1563.

[39] Holcomb, D.J. and Costin, L.S., 1986. Detecting damage surfaces in brittle materials using acoustic emissions.

[40] Walsh, J. and Brace, W.F., 1964. A fracture criterion for brittle anisotropic rock. Journal of Geophysical Research, 69(16), pp.3449-3456.

[41] Schulson, E.M. and Hibler III, W.D., 1991. The fracture of ice on scales large and small: Arctic leads and wing cracks. *Journal of Glaciology*, *37*(127), pp.319-322.

[42] Danzer, R., Lube, T., Supancic, P. and Damani, R., 2008. Fracture of ceramics. Advanced engineering materials, 10(4), pp.275-298.

[43] Wang, H. and Singh, R.N., 1994. Thermal shock behaviour of ceramics and ceramic composites. *International Materials Reviews*, *39*(6), pp.228-244.

[44] Guiu, F., Reece, M.J. and Vaughan, D.A.J., 1991. Cyclic fatigue of ceramics. *Journal of materials science*, *26*, pp.3275-3286.

[45] Pelleg, J. and Pelleg, J., 2017. *Creep in ceramics* (pp. 41-61). Springer International Publishing.

[46] Kostrov, B.V., 1974. Crack propagation at variable velocity: PMM vol. 38, n≗ 3, 1974, pp. 551–560. *Journal of Applied Mathematics and Mechanics*, *38*(3), pp.511-519.